CAAP Final Report

Date of Report: 12/5/2018

Prepared for: *U.S. DOT Pipeline and Hazardous Materials Safety Administration*

Contract Number: DTPH5615HCAP04L

Project Title: An Inorganic Composite Coating for Pipeline Rehabilitation and Corrosion Protection

Prepared by: Hao Wang, PhD; Milad Salemi; Jiaqi Chen, PhD; P.N. Balaguru, PhD; Jinhao Liang; Ning Xie, PhD

Contact Information: Hao Wang, PhD, Department of Civil and Environmental Engineering, Rutgers, The State University of New Jersey

An Inorganic Composite Coating for Pipeline Rehabilitation and Corrosion Protection

Table of Contents

Chapter 1 Introduction

1.1 Background

The pipeline system is one of the most capital-intensive infrastructure systems. The structure integrity of pipelinesis decreasing due to corrosion. Corrosion failures can be either leaks or ruptures that could cause pipeline safety hazards. Pipelines are also susceptible to erosion and mechanical damage. Another form of degradation is stress corrosion cracking (SCC) or corrosion fatigue (Fessler 2008). These pipeline degradations cause high maintenance costs and result in the adverse consequences and the interruption to product transportation and distribution.

The process of corrosion begins due to the electrochemical reaction of a surface with corrosive environment. One common strategy is to effectively isolate a substrate's surfaces from electrochemical (corrosive) attack by covering it with a protective coating. The selection of coating depends on pipeline terrain, soil conditions, joint coating solutions, electrical-resistance stability, pipeline operating temperature, and lifetime cost among others. Among different coatings, organic coatings, such as fusion bonded epoxy have been commonly used. However, conventional coating systems all have limited field service life.

The pipeline coating should resist damage to impact, gouge, and abrasion due to pipe movement and retain adhesion under harsh environments. Concerns arise when the coating layer is mechanically damaged during installation, transport, or operation. Organic coatings are susceptible to damage by surface abrasion and wear and have relatively poor resistance to the initiation and propagation of cracks. This may introduce localized defects in the coating and impair mechanical strength. The defects can also act as pathways accelerating the ingress of water, oxygen and aggressive species onto the metallic pipeline, resulting in localized corrosion.

On other hand, the aging and degradation of pipeline system induces the need of cost-effective repair techniques such as fiber reinforced composite for ease of installation and application against adverse environmental effects. Fiber reinforced composites could provide excellent advantages in terms of weight, cost, moisture and chemical resistance, toughness, abrasive resistance, and strength. The applicability of composite overwrap repairs to pipelines has been advocated by the American Society of Mechanical Engineer (ASME) for the possible repair scenarios of hoop, axial and leak proofing (ASME 2006). The repair of corroded pipelines with fiber reinforced composite materials is getting more applications in the pipeline industry.

In recent years, numerical analysis and experimental studies on sandwich and layered composite applications have shown that fiber-reinforced composite repairs are effective for pipelines with external corrosion defects (Alexander and Francini 2006; Sen and Mullins 2007). Fiber composite materials also provide excellent advantages over other repair technologies by providing additional corrosion mitigation and improving resistance to blast, explosion, and fire.

1.2 Objective

Coatings are used to steel pipelines against hostile environmental conditions such as exposure to corrosive chemicals, moisture ingress, ultra violet (UV) radiation, etc. The proposed project aims

to address the need for an inorganic coating composite for corrosion protection of pipeline in aggressive environment. The inorganic coating does not generate CO_2 emission or volatile organic content (VOC). Inorganic coatings are frequently used in construction industry as anti-corrosion coatings, which are effective, chemically inert, hard, and thermally stable. In this study, microfiber reinforcement and nano-modification were used to improve the performance of inorganic coating system. The research work integrates both laboratory testing and numerical simulations. The major tasks conducted are: 1) development of inorganic coating with nano modification; 2) accelerated corrosion testing; 3) durability and adhesion strength testing; 4) shear testing of coating with carbon fiber reinforced polymer (CFRP); and 5) analytical study of composite repair system of pipeline.

The high-strength inorganic coating matrix can form strong bonding with the pipeline surface. It is expected that the fiber-reinforced coating composite will strengthen the metallic pipelines undergoing elastic or inelastic deformation with localized corrosion or mechanical damage that impair the serviceability. Once applied, the high-strength coating will not be damaged in handling during construction or in operation by soil stress or soil movement and thus provide protection in the long run.

Chapter 2 Literature Review

2.1 Pipeline Coatings for Corrosion Protection

2.1.1 Pipeline Corrosion

Two corrosion patterns exist in natural gas pipelines: internal and external corrosion. Most internal corrosion happens in wet pipelines, especially in the hazardous liquid pipelines. Water or other liquid materials, such as aqueous, may cause the corrosion reaction through providing electrolytes. Bacteria will be formed in the process and contaminate the internal environment of pipeline. Baker (2008) reported that carbon dioxide or hydrogen sulfide, which could form acid in the gas pipeline and cause corrosion inside the pipe due to the import of liquid from the wells.

External corrosion occurs due to environmental conditions outside of the pipe.Majid et al. (2010) explained that erosive slurry was formed by the combination of soil and sand, which highly influenced the metal loss of pipes. Alrudayni (2015) stated that the finer soils such as silt soil or clay could result in more corrosive earth environment than the coarser soils like sand and gravel due to the difference in electrical conductivity. Basically, finer soils have high moisture content, poor drainage, and high salt content. Heavy clay soil can result in deterioration of the pipe's due to the adhesive force with the change of moisture content. Therefore, soil conductivity, the reversed results of soil resistivity, has close relationship with corrosion rate, as shown in Table 1. There are many additional factors that accelerate the formation of aggressive soil environment such as the level of CP, mixed dissimilar soil types, complicated alloys, groundwater table variations, pH level, etc.

Table 1 Soil resistivity effect on corrosion rates (Adapted from Alrudayni 2015)

Soil Resistivity (Ohm-cm)	Soil Type	Moisture	Corrosion Rate (mm/yr)
<500	Muskeg/sloughs/free water accumulation	Always wet	Very corrosive >1.0
500-2000	Loams/clays	Mainly wet	Corrosive to moderately corrosive 0.5-1.0
2000-10000	Gravels, sandy	Mainly dry	Mildly corrosive 0.2-0.5
>10000	Arid, sandy	Always dry	Noncorrosive <0.2

From the theoretical perspective, corrosion is caused by an electrochemical reaction due to aggressive environmental effects such as soil, moisture exposure, chemical products (chloride ions or sulfates), and some pollutants (bio-bacteria) (Alrudayni 2015). According to Weiser (2011), metal corrosion can be divided into bimetallic corrosion and holiday corrosion. Holiday means a small hole or a defect in a disbonded coating (Song and Sridhar 2008). The first type of corrosion process is the result of ion loss from one part of metal to another through metal transmission. The second is more common for buried pipelines, which shows that the difference in oxygen concentration can be manifested as energy difference resulting in a potential difference, while it is electrically connected by electrolyte (water). The areas in the pipe with the lower oxygen

concentration (inside the crevice) function as an anode and the areas with higher oxygen concentration such as loam function as a cathode (Alrudayni 2015).

2.1.2 Pipeline Coating

The function of coating system is to isolate the contact between steel and electrolyte. Environmental effects, such as ultraviolet (UV) degradation, moisture ingress, operation temperature, and chemical resistance of the soil, are the major factors affecting the long-term performance of the coating system of buried pipes.

An effective coating requires high resistance to chemical agents, bacteria, abrasion, impact, and temperature. A multi-layered coating system is usually adapted, including primer and topcoat. Coatings can be made using organic, inorganic, and metallic materials, which provide specific functions (Popoola et al. 2014). Metallic and inorganic coatings could provide barriers for metal substrates. Metallic coatings are applied by electrodeposition, flame spraying, cladding etc. Inorganic coatings are applied by brushing by hand or spraying by machine. The metal coating forms sacrificial layer and creates passive oxidation with the soil environment to protect the steel. The pipes currently used in the market have been coated with extruded polyethylene or polypropylene plastic coating, coal tar enamels, mastics, and epoxy.

Schad and Zipfell (2007) discussed a variety of corrosion protective systems, such as tapes, shrink sleeves, and liquid coatings. Polyethylene (PE) factory coatings are electrical high isolating, nearly impermeable to vapor and oxygen, which are cost effective and flexible to temperature changes. Duroplast coatings are good for irregular shaped or already installed objects, since they are viscous fluids during application. Cool tar and bitumen coatings are old types of coatings and have many issues such as brittleness which results in cracks and decreased adhesion to steel surface and have poor electrical insulation resistance. They also contain sulfide that causes bacteria and penetrates into crevices in coating. Therefore, coal tar and bitumen coatings should not be used. On the other hand, field coatings should be easy to apply and have tolerability to applications. There are thermoplastic and thermosetting coatings for warm and cold applications. They do not need to withstand the same mechanical resistance as factory coatings since they avoid transport and loading defects that happen in factory coatings.

Conventional chromate conversion coatings (CCC), also known as, chromium-based coatings, have been replaced by sol-gel films because their toxicity makes them threat to human health and safety. For corrosion protection, the sol-gel techniques mixed with the layer-by-layer (LBL) method works for creating a barrier film. LBL films can work together with organically modified silica layers, which will achieve corrosion protection similar to that provided by chromate coatings. The use of zinc as coating is also not encouraged due toits significant price fluctuations (Popoola et al. 2014).

The assembled nanophase particle process creates a coating with long-term coating performance and exceptional corrosion resistance that works as physical barrier against corrosion. However, it lacks the ability to release corrosion inhibitors. He and Shi (2009) developed a self-repairing anti-corrosion primer coating by using cage-like smart particles to reserve repairing agents and release them in a controllable way. In this process, when defect occurs, nano-reservoirs release both

repairing agent and catalyst. The technology is also practicable for inorganic coatings. Self-repairing primer coatings are also feasible and can be environment- friendly alternatives to CCCs.

An epoxy coating is another good option for corrosion protection, as epoxy has outstanding electrical insulation properties and strong adhesion strength. Epoxy can work as reservoir and has properties similar to those of self-repairing primer that allow it to release the inhibitor. Mixing inorganic filler particles into epoxy coting can form nanocomposite that will create coating with enhanced durability. The major function is to shield the metal surface. Combining the three nanoparticles of Fe_2O_3, SiO_2, and halloy site clay can greatly improve anti-corrosion and mechanical properties of coating through changing the internal microstructure such as density and void volume (He and Shi 2009).

Zhang et al. (2012) introduced potassium aluminosilicate coating known as geopolymer and inorganic coating for chemical corrosion. These were used primarily for marine concrete structures. The anti-corrosion property of geopolymer coating is influenced by its microstructure. The humidity and the thickness of coating layer were found being two main factors that affected the performance of a geopolymer coating. The existing shrinkage problems can be solved by adding polypropylene (PP) fiber and MgO.

In the recent study conducted by Federal Highway Administration (FHWA), the coatings that were analyzed included three-layer systems consisting of organic, inorganic, and moisture-cured zinc-based primers; two-layer systems with various combinations of zinc-based primers and organic top coats; and single-layer system of calcium sulfonate alkyd. Cyclic corrosion testing was concluded due to its low cost and quick results. The results of pull-off strength testing showed that the two-layer coating, thermally sprayed zinc primer/ linear epoxy (TSZ/LE) and experimental zinc primer/ linear epoxy (ZnE/LE), had poor adhesion strength compared to initial data, while the three-layer coatings, Inorganic zinc-rich epoxy / epoxy / aliphatic polyurethane (IOZ/E/PU) and zinc-rich epoxy primer/ epoxy / aliphatic polyurethane (ZE/E/PU), exhibited greater adhesion strength performance. Although the integral performance of High-ratio calcium sulfonate alkyd (HRCSA) was excellent, the adhesion strength was far below that of two-layer and three-layer systems (Kodumuri and Lee 2012).

2.2 Corrosion Test Methods

ASTM B117

The ASTM B117 specification is the oldest and most widely used international standard for interpreting the results of salt fog test. The total testing period could be 24 to 5,000 hours with 24-hour increments, depending on the demands of the structure's service life. The coated or uncoated metal samples are placed on a wooden frame in an enclosed chamber in the slant of 15 to 30 degree from the vertical. The samples should be repositioned daily. ASTM D1193 provides the specification for the reagent water. Sodium chloride solution is regulated to be 5 percent and pH value should be between 6.5 and 7.2. Prior to placing the samples, the chamber should be preheated to 95°F (35°C). It is noted that ASTM D5894 test uses combined solution of sodium chloride and ammonium sulphate, which is more like industrial purpose.

Cyclic Corrosion Tests

Claydon (n.d.) summarized cyclic corrosion tests (CCTs) adopted by different codes, as shown in Table 2. These CCTs vary in salt fog period, dry or freeze period, and UV/ condensation period. The ISO 230240 test performed well to simulate thermal temperature gradient. The smaller gradient of -20℃ C to 60℃ C took into consideration low temperature condition. However, the first three methods did not consider freeze condition. Therefore, they are not applicable for buried condition at cold environment. The CCTs have more accurate simulation of field performance than do the traditional salt fog tests (ASTM B117, ISO 7253), which has been documented by many corrosion institutes and industry associations over the past 5 -10 years.

Table 2 Accelerated salt fog test in different codes

Norsok Cyclic Test (based on NACE TM0184)	72 hours Salt Fog (ASTM B117, ISO 7253) with artificial sea water (ASTM D1141)/ 16 hours dry (23℃)/ 80 hours UV at 60℃/condensation at 50℃, 4 hours/ 4 hours cycle (ASTM G53) Total duration = 25 weeks
ASTM D5894	168 hours Prohesion (ASTM G85, Annex A5)/ 168 hours UV at 60℃/condensation at 50℃, 4 hours/ 4 hours cycle (ASTM G53) Total duration = 24 weeks
Draft NACE (Based on Shell)	168 hours Prohesion (ASTM G85, Annex A5) with artificial sea water (ASTM D1141) 168 hours UV at 60℃/condensation at 50℃, 4 hours/ 4 hours cycle (ASTM G53) Total duration = 12 weeks
Draft ISO 23040	72 hours Salt Fog (ASTM B117, ISO 7253) / 24 hours freeze at -20℃/ 72 hours UV at 60℃/condensation at 50℃, 4 hours/ 4 hours cycle (ASTM G53) Total duration = 25 weeks

ASTM-D4587

The ASTM D4587 specification provides the test cycles for fluorescent UV-condensation exposure. The required cycle durations, radiation irradiance, and black panel temperatures for different coating applications are illustrated in Table 3.

Table 3 Test cycles for different coating applications (ASTM D4587)

Cycle Number	Cycle Description	340 nm Irradiance	Black Panel Temperature	Typical Uses
1	8 h UV 4 h condensation	0.83 W/(m^2·nm) Dark period	70 ± 2.5℃ (158 ± 5℉) 50 ± 2.5℃	Automotive coatings

	Repeated continuously		(122 ± 5°F)	
2	4 h UV 4 h condensation Repeated continuously	0.89 W/(m^2·nm) Dark period	60 ± 2.5°C (140 ± 5°F) 50 ± 2.5°C (122 ± 5°F)	Industrial maintenance coatings
3	4 h UV 20 h condensation Repeated continuously	0.89 W/(m^2·nm) Dark period	60 ± 2.5°C (140 ± 5°F) 50 ± 2.5°C (122 ± 5°F)	Exterior wood coatings
4	8 h UV 4 h condensation Repeated continuously	0.89 W/(m^2·nm) Dark period	60 ± 2.5°C (140 ± 5°F) 50 ± 2.5°C (122 ± 5°F)	General metal coatings

FHWA-HRT-12-044

In the corrosion test conducted by FHWA (Kodumuriand and Lee 2012), the length of the accelerated laboratory testing (ALT) will be 7200 hours for 20 cycles. The test cycle will be one hour wet/ one hour dry. In the wet cycle, a Harrison mixture of 0.35% (wt) ammonium sulfate and 0.5% (wt) sodium chloride was used. In the dry cycle, the chamber temperature was set at 95 °F (35 °C). The cycle details were summarized in Table 4.

Table 4 Corrosion Test Method Used by FHWA Study (Kodumuriand and Lee 2012)

Total Cycle	20
One Cycle	360 h
Freeze	24 h at -10°F
UV/condensation	168h
Test Cycle	4 h UV/4 h condensation cycle
UV lamp	UVA-340 nm
UV temperature	140°F (60°C)
Condensation temperature	104°F (60°C)
Prohesion Exposure	168h

2.3 Pipeline Repair Technology

2.3.1 Traditional Pipeline Repair Methods

The traditional approach of pipeline repair is to cut off the damaged segments and replace with new substitution. Fillet-welded patches, which are attached to the external surface of the defective section, perform well in addressing local flaws. Flush-welded patches do the same job but they only cut off the flawed area around the damaged section, and the edge is required to be rounded. At present, full encirclement steel sleeves, welded leak boxes, and steel mechanical clamps are widely used. For the sleeve method, the Type A sleeve is used for locally corroded pipe, and no

weld is required. The Type B sleeve is for cracked pipes and the two ends should be closure welded.

2.3.2 Composite Repair

The composite rehabilitation method that is currently used to restore deteriorated pipes is the FRP matrix composite overwrap system. The structure of FRP system includes several layers of fiber composite laminates, an epoxy bonding layer, and filler in the defect. Existing codes and standards for composite repair, such as ASTM D 2992, ASME PCC-2-2006 (Part 4), ISO 24817 and ASME B31.4, provide important guidance (Shamsuddoha et al. 2012). Resin plays a significant role in the composite repair system and it can be epoxy, polyester, vinyl ester, phenolic, polyurethane, etc. Epoxy resin and polyurethane are very common in the application.

The FRP repair system offer three advantages. First of all, it requires shorter time and lower maintenance cost. Second, the potential risk of explosion is eliminated. Third, no gas or liquid products suffer losses and pipelines can keep operating during the rehabilitation process. Additionally, the external corrosion is restricted by FRP through covering the exposure surface to avoid admitting corrosion agents. The wrap has been proven to prevent seismic failure due to its remarkable confinement ability (Kash 2003). It was reported that the former old approaches (traditional clamps and sleeves) were about 20% more expensive than FRP system and the latter one (replace) was around 70% more costly (Duell et al. 2008). Although the FRP is an emerging composite system, the rate of FRP use is still low. The steel sleeves method still dominates the market. However, the rate of intention to use the composite repair technique is higher than that of other methods (Farrag 2013).

Glass fiber and carbon fiber are favored in most cases of composite repair system. Glass fiber is a low-cost material that is easy to integrate with resin layers and able to inhibit chloride ions, but it is prone to stress rupture, creep, and fatigue, as well as sensitive to high temperatures (Kash 2003, Shamsuddoha et al. 2012). Compared with aramid and glass fiber, carbon reinforced polymer can endure higher internal pressures. The direct contact between carbon and steel surface in the submerged condition will generate galvanic corrosion. However, for the buried condition, the effect may be insignificant. To eliminate the corrosion, a hybrid composite system that uses glass-fiber-covered carbon fibers can be used (Shamsuddoha et al. 2012).

Duell et al. (2008) introduced multi-layer FRP repair system with high strength carbon fiber wraps and adhesive epoxy material with high-speed curing. The composite wrap was around 0.122-in. thick. Putty material, diglycidyl ether of bisphenol A (DGEBA)-based epoxy cured with aliphatic amine hardener and thixotropic fumed silica additive, were used for filling the defective part to restore the original shape of pipeline. The carbon fiber material was woven with 12000 and 6000 tows in the warp and the fill direction, respectively, which was used together with epoxy. The tow means the number of carbon filaments in each bundle. Three defect geometries were machined to be 1”by 6”, 3” by 6”, and 6” by 6”, respectively. The defect depth was 50% of the wall thickness. Epoxy putty filled the defects and woven carbon fiber wraps covered the repaired surface. Epoxy-based composite fibers were cured for 24 hours. The pipe was tested through pressurizing under hydraulic power. Finite element simulation software was used to simulate the FRP model. The metal material parameters adopted Mises yield theory and the associated flow rule. The putty

properties were modeled with elastic stress-strain behavior. Both experimental and simulation results proved the effectiveness of FRP repair system.

Égert and Pere (2009) simulated the FRP system using multilayered elastic shell model and three-dimensional (3-D) solid model. The multilayered repair system was applied both internally and externally. The 3-D model considered the round corner that the shell model could not simulate. Metal materials and PE were modeled as linear elastic material, accounting for modulus of elasticity, Poisson's ratio, yield strength, and tensile strength of the materials. The results showed that the highest deformation occurred in the tangential direction for the internal case and occurred at the center for the external case. However, the strain and stress were similar. In addition, relatively few CFRP layers were found to be sufficient for the repair system. The performance of two plies and four plies was the best as too many composite layers could result in weaker strength. The shell model was found sufficient to conduct the simulation and it required less work.

Mally et al. (2013) evaluated composite repair system that was installed and cured while submerged to investigate the impact of aqueous submersion on material behavior. Full-scale testing on three pipe geometries, straight, elbow, and tee were conducted. The performance of composite repair that was installed while submerged was found comparable to the performance of the composite installed on dry substrates for the complex geometries. For the straight geometries, repair failure pressures were lower in the immersed state, but were still above the design pressure. Underwater installation resulted in statistically significant reduction in burst pressures for straight pipes due to poor interfacial bonding, not reduced composite mechanical.

Chan et al. (2014) investigated numerical models and experimental data for a fiber-reinforced PE strip repair system. ABAQUS software was used in the modeling procedure. The model contained two parts: the epoxy grout with the external surface of the corroded steel surface, and PE strips and epoxy grout within curing. The steel material was defined by the stress-strain relationship and adopted Ramberg-Osgood material model. The material properties considered Young's modulus of steel, Poisson's ratio, yield stress, yield offset, and the hardening exponent of the Ramberg-Osgood model. The difference between the FEM and the ASME code was found less than 10%. The difference between the test and the FEM was smaller than 6%. The results of FEM were more conservative than the industrial standard.

2.3.3 Patch Repair vs. Full Encircle Repair

Smaller patch-type repair has become an alternative in the composite repair options, which was developed to decrease the cost in equipment application, labor, and material for the increasing demands of large pressure piping. The novel improvement also depended on the improved capability on the wrapping composite repair. However, this methodology is not given in ASME PCC-2. Compared with fully encirclement repair, only specific area is required to make up due to less preparation for the surface's sanding and blasting.

Since the defect geometry has significant impact on the remaining strength of corroded pipeline (Cunha and Netto 2012), the full wrap repair strategy could be conservative for some small and shallow defects. In this case, the application of patch repair could be feasible. Moreover, with a

pre-cured FRP patch, the time consumption for the repair could be further reduced. However, the load transfer mechanism and mechanical behavior of the FRP patch repair is still unclear.

Theisen and Keller (2016) conducted finite element simulation and experimental tests for both patch and wrap repairs on through-wall defects. The 2.4-inch overlap extending along axial and circumstantial direction is required by ASME PCC-2 and used in the simulation. The simulation showed that the max strain of patch was slightly higher than the one of wrap type. Approximately 29.4% difference was found at internal pressure of 500 psi. Simultaneously, the average fatigue life for patch repair was also slightly higher than the one for full encircle repair. The overlap length should satisfy the standard (ASME PCC-2) and cannot unlimited extend the defect depending on the size and material.

Ayaz et al. (2016) studied the composite patch repair with different thicknesses and overlap lengths in different directions. A patch was used to repair a small through-wall hole. FEM model was simulated and analyzed. The results showed that the increment in overlap length could enhance the failure strength as well as the angle and thickness could generate internal pressure.

Ramakrishna and Balu (2017) conducted a comparative study in FEM simulation that shows the symmetric rectangular shape will be the most effective when compared with elliptic and circular repair.

Chapter 3 Preparation of Nano-Modified Inorganic Coating

3.1 Development History of Inorganic Composite Coating

The composite coating formulations were further developed from an inorganic polymer developed in a previous study (Papakonstantinou and Balaguru 2007). The earlier study resulted in the development of an alkali-alumino-silicate system that can be used for high strength composites using various high strength fibers including carbon fibers (Najm et al. 2007; Toutanji et al. 2006).

A number of field demonstration applications were carried out in early studies. The durability of coating system on concrete was successfully tested with 100 cycles of wetting-drying and 50 cycles of freezing-thawing. There was no degradation of the coating or the interface. The oldest coated surface is performing well after 20 years in service (Balaguru and Lee 2001). The maintenance crew was able to apply the coating with minimum training. This composition is more economical than most other coatings and has been used in a number of field-demonstration applications on concrete surfaces.

The inorganic coating formulation used in this study is potassium alumina-silicate, or polysialate-silox with the general chemical structure:

$$K_n\{-(SiO_2)_z-AlO_{2-}\}_n \bullet wH_2O$$

Where, $z>>n$ and n is the degree of polycondensation; z is 1, 2, and 3; and w is the binding water amount.

The specific features of inorganic composite coating include:

- The resin is prepared by mixing a liquid component with a potassium-poly (sialate-siloxo) powder to plastic consistency with the resulting mixture referred to as matrix. Fillers and hardening agents can be added to the powder component to enhance matrix properties.
- 100% inorganic nature without any volatile organic component (VOC)
- The matrix is water-based; consequently, tools and spills can be cleaned with water. All of the components are nontoxic and no fumes are emitted during mixing or curing.
- Common application procedures such as brushing, rolling and spraying are compatible with the matrix.
- The base coating material is white and hence other color schemes can be easily formulated using pigments.
- The system is compatible with brick, concrete, wood, and steel.
- Micro-fiber can be added to control shrinkage cracking and provide high abrasion resistance
- The coating will not undergo any change up to temperature of 800ºF. Organic coatings could soften at temperatures less than 150ºF.

Lyon et al. (1997) found that geopolymer composite is non-combustible, while all of the organic polymer matrix combustion supports flaming combustion. Difference in the initial strength of organic matrix and geopolymer resin composites can be compensated in the design phase of a structure by modifying the dimensions of the structural element, but the residual strength of a fire exposed composite structure is determined by physical dimensions, thermal transport properties, material chemistry, and thermal stability of the composite. The geopolymer is superior with regards to specific modulus and its high temperature structural capability and fire resistance.

Though, its flexural strength, modulus, and cost is not as favorable as structural steel, it has superior temperature capability.

Balaguru and Chong (2005) discussed the postponing of failure in concrete using inorganic and organic matrix with carbon fiber. The organic matrix provided higher deformations at failure, but the organic matrix failed by delamination. The benefits of inorganic matrix were that it is fire and UV resistant. Inorganic matrix composite developed micro cracks and failure occurred by fracture of carbon. The load transfer played an important role in the repair design of concrete. The load transfer from fiber to fiber within the composite plate is not very efficient, especially when fiber areas are large. For both organic and inorganic matrices, the average fiber strain at failure reduced with the increase in fiber area. Since carbon composites were used to strengthen unreinforced systems, load redistribution through cracks plays major role in the failure mechanism.

Balaguru and Brownstein (2008) studied inorganic protective coatings and fiber reinforced polymers for repair and rehabilitation of transportation structures. The composite was inorganic, and resistant to fire and UV, water-based, and had no toxic substances. The matrix cured to glassy texture and therefore was graffiti resistant surface. The study concluded that the inorganic polymer coating was used successfully for coating deteriorated concrete surfaces. Both inorganic and organic polymer based composites can be used successfully to protect and seal junctions made with different construction materials.

3.2 Preparation of Coating with Different Nano-additives

There are different nanomaterials available for coating modification. Nanomaterial can be made of metals, semiconductors, oxides or carbon materials. Nanomaterial is defined as materials which have structured components with at least one dimension (e.g. grain size, diameter of cylindrical cross-section, layer thickness) less than 100 nm. Nanomaterials are usually classified into three categories depending on their geometry: nanoparticles, nanotubes, and nanosheets. Since a wide variety of synthesis methods have been used in production, nanofillers may differ greatly in diameter, aspect ratio, crystallinity, crystalline orientation, purity, entanglement, surface chemistry, and straightness. The selection of nano-modification should consider the cost, preparation method, and the effectiveness on corrosion resistance.

It is hypothesized that the mechanisms of the nano modification for corrosion protection on steel substrate are mainly from two aspects: 1) from microstructure perspective, the nanoparticles improved the quality of the inorganic coating, reduced the porosity of the coating matrix, and thus zigzag the diffusion path of the deleterious agents. As a result, it will improve the corrosion resistance of the inorganic coatings; and 2) the addition of the nanoparticles can improve the bonding strength of the cured inorganic coating to the steel substrate and altered the physical and chemical properties of the coating-steel interface.

The first set of steel coupons was prepared with different nano-materials to identify the most promising modifier from various materials. The coating samples were prepared with different nano-additives, including titanium oxide, iron oxide, zinc oxide, nanoclay, silicon dioxide, in addition to the control sample. The nano-particles were ultrasound in the water for four hours before mixing with the coating matrix. The coating was prepared by mixing the liquid component,

powder, and water that was dispersed with nano-particles to have plastic consistency. After that, coating was applied on steel coupon with a foam brush. In addition, polyvinyl alcohol (PVA) was used to substitute partial content of water in the mix that produces another formulation of geopolymer matrix. The coatings were applied in three layers after the proper curing (24-48 hours) was achieved for each layer. The total coating thicknesses were found being around 400 micrometers (16 mils). Figure 1 shows the pictures of steel coupon, brush, and nano-modified coating.

The second set of steel coupons was prepared with three different nanomaterials (titanium oxide, iron oxide, and silicon dioxide) to further investigate the effectiveness of nano-modification. The nanoparticles were purchased in two different formats: powder and dispersion in water. For the nanoparticles purchased in powder, the dispersion and mix procedure described above was used for dispersion. For the nanoparticle purchased in solution, the liquid component, powder, solution, and water (reduced amount due to water in the solution dispersed with nanoparticles) were mixed together directly. After that, coating was applied on steel coupon with a foam brush. The coatings were applied in three layers after the proper curing (24-48 hours) was achieved for each layer. The total coating thicknesses were found being around 160-200 micrometer (6-8 mils).

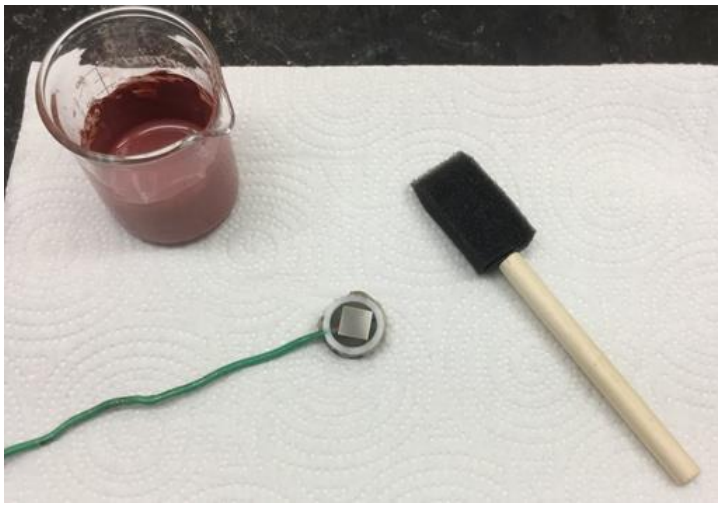

Figure 1 Steel coupon, brush, and nano-modified coating

3.3 Electrochemical Impedance Spectroscopy Testing

Electrochemical measurements were conducted using Electrochemical Impedance Spectroscopy (EIS) testing following the specification of ASTM G3-14 *Conventions Applicable to Electrochemical Measurements*. This technique involves applying small-amplitude alternating current signal into the material over a wide range of frequencies and measuring the responding current and its phase angle shift. The EIS provides an attractive way in terms of allowing rapid determination of corrosion rate and revealing information pertinent to corrosion mechanism. It is a good approach to compare the relative performance of different coatings. However, electrochemical techniques generally give information on the instantaneous corrosion rate and may not predict the long-term corrosion behavior in the field environment.

EIS measurements were conducted using a three-electrode system, as shown in Figure 2. The coated steel coupon served as the working electrode, while the counter electrode and the reference electrode used were a platinum grid and a saturated calomel electrode (SCE), respectively. The corrosive environment was provided by 0.3% aqueous NaCl solutions. The EIS measurements were carried out using Gamry Reference 600 device, which is high-performance, research-grade potentiostat/galvanostat/ZRA designed for fast and low-current measurements. The steel was polarized at ±10 mV around its open circuit potential (OCP) by an alternating current (AC) signal with its frequency ranging from 300 kHz to 5 mHz (10 points per decade).

Figure 2 EIS testing with coated sample

Potentiodynamic tests were conducted using EIS to measure polarization resistance following the specification of ASTM G59. The corrosion potential, corrosion current density, and anodic /cathodic Tafel slope were derived from the data. Based on the approximately linear polarization behavior near open circuit potential (OCP), polarization resistance values were derived from Stern-Geary equation, as shown in Equation (1). Polarization resistance can be related to the rate of general corrosion for metals at or near their corrosion potential. Polarization resistance measurements are an accurate and rapid way to measure the general corrosion rate.

$$AR_p = \frac{b_a b_c}{2.303 i_{corr}(b_a + b_c)} \quad (1)$$

Where, R_p is polarization resistance; i_{corr} is corrosion current density; and b_a and b_c are anodic/cathodic Tafel slopes.

Figure 3 compares the polarization resistance of the first set of coating samples with various nano-additives after different immersion periods (0-8 days). The results showed that the incorporation of nanoparticles increased the corrosion resistance of the inorganic coatings at different degrees. In general, silicon dioxide and iron oxide showed better corrosion resistance than the control sample and the other nano-modified samples, especially after several days of immersion. This could be caused by the secondary reaction when the coating sample was immersed in the NaCl solution. The reaction product could reduce the porosity of coating matrix and increase corrosion resistance.

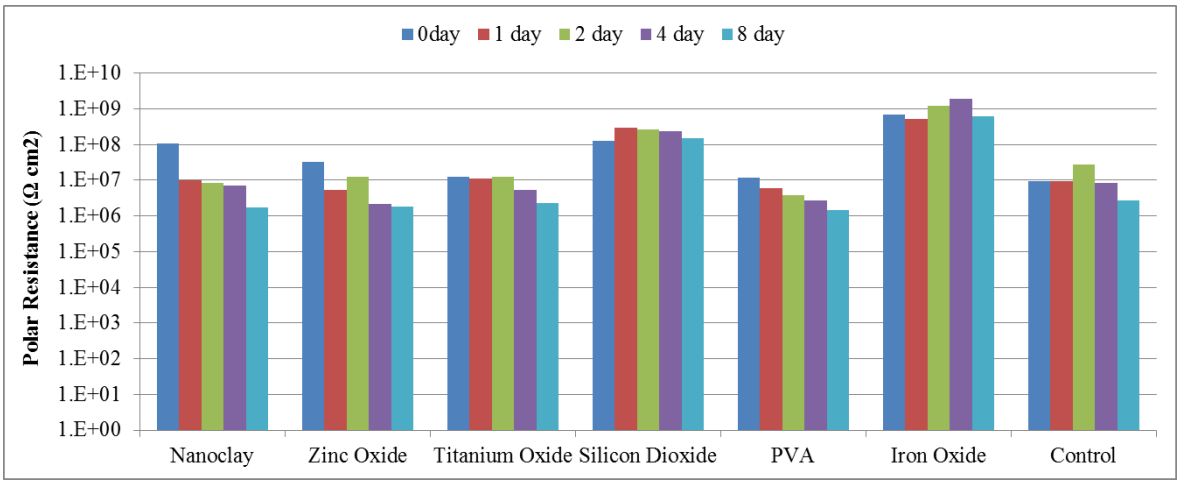

Figure 3 Polarization resistance of the first set of coating samples with various nano-additives after different immersion periods

The EIS testing results in Nyquist curves of the second set of coating samples were shown in Figure 4, respectively, for different immersion periods (2 days and 4 days). Figure 5 compares the polarization resistance of the second set of coating samples. The electrochemical measurements showed that the incorporation of nanoparticles increased the corrosion resistance of the inorganic coatings at different degrees. However, variations were observed in corrosion resistance as the soak time increases.

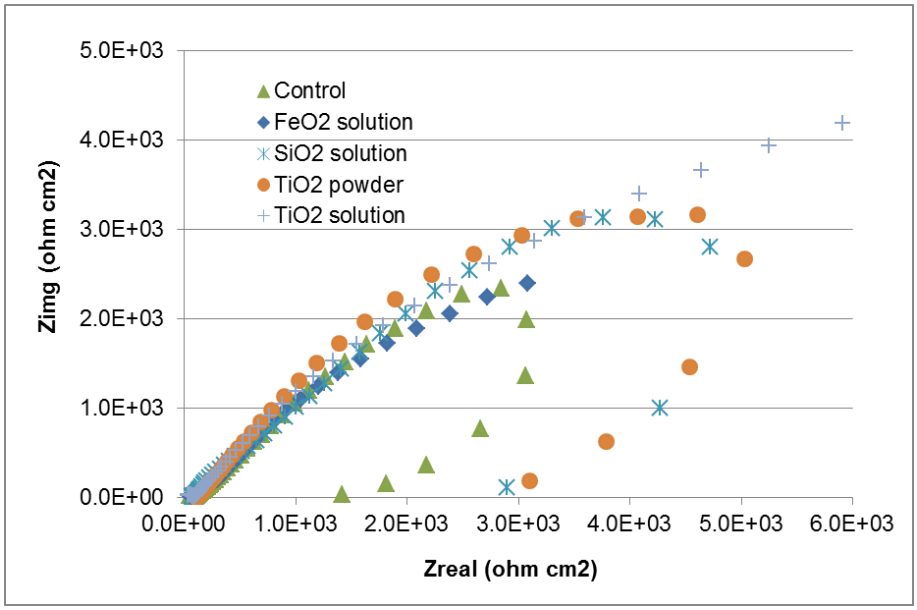

(a)

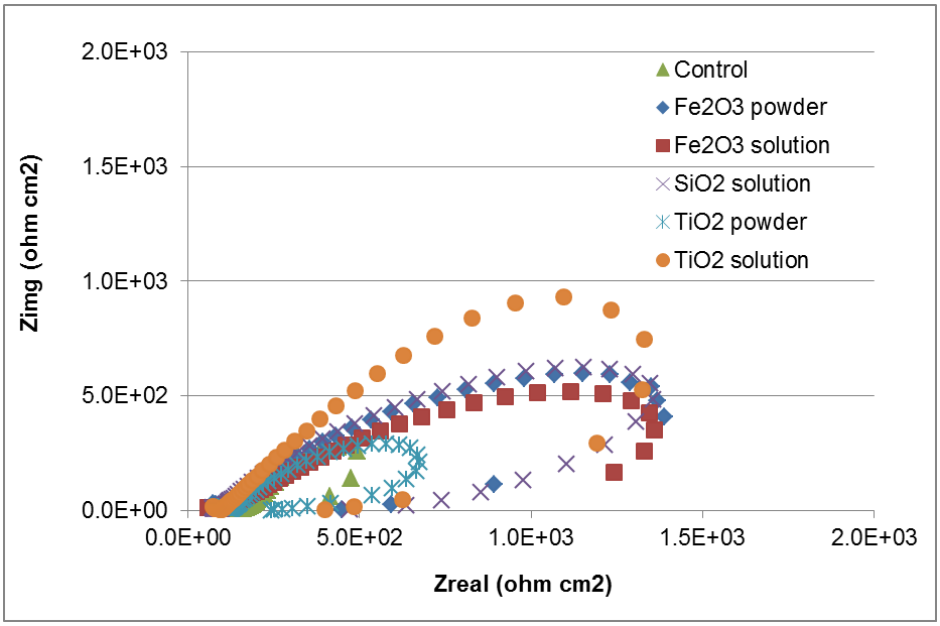

(b)

Figure 4 Nyquist curves of nano-modified coatings after immersion of (a) 2 days; and (b) 4 days

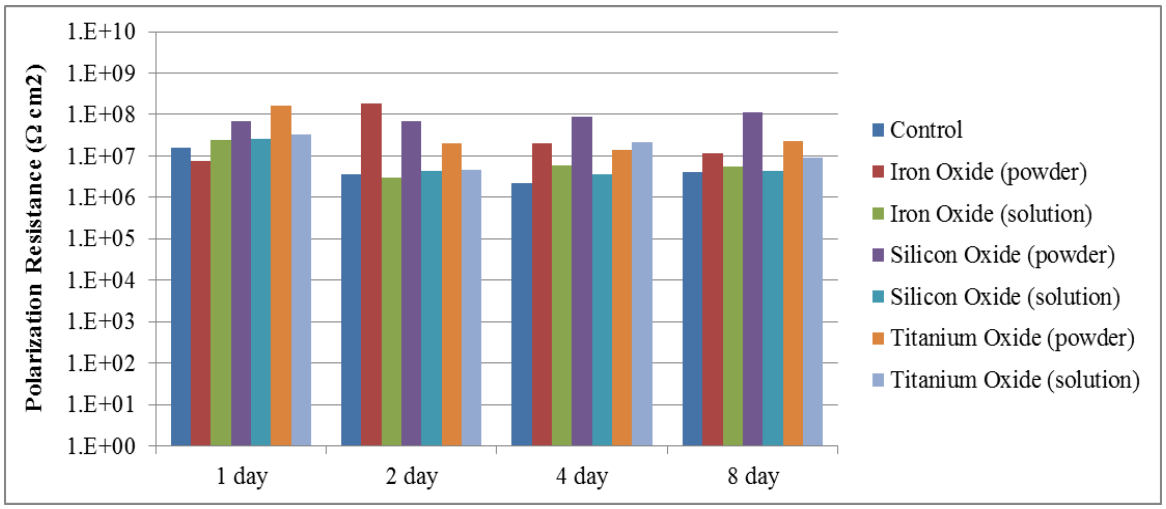

Figure 5 Polarization resistance results of the second set of nano-modified coating samples after different immersion periods

Chapter 4 Durability and Adhesion Testing of Coating

4.1 Accelerated Corrosion Testing Environment

An accelerate corrosion testing environment is set up for study of coating durability. The following reference document was first reviewed for developing an accelerated corrosion testing procedure in this study.

- ACE TM0169/ASTM G31 - Standard Guide for Laboratory Immersion Corrosion Testing of Metals
- ASTM B117 - Operating Salt Spray (Fog) Apparatus
- ASTM G85 - Standard Practice for Modified Salt Spray(Fog) Testing
- ASTM D1654 - Evaluation of Painted or Coated Specimens Subjected to Corrosive Environments
- ASTM – D4587 Standard Practice for Fluorescent UV-Condensation Exposures of Paint and Related Coatings
- FHWA-HRT-12-044 FHWA 100-Year Coating Study
- Chong, Shuang Ling. "A Comparison of Accelerated Tests for Steel Bridge Coatings in Marine Environments." Journal of Protective Coatings & Linings, vol. 14, no. 3, 1997

A custom corrosion chamber was built to achieve an accelerated corrosion process, as shown in Figure 6. The components of the chamber include the following:

1. A 100 Gallon chamber (tank)
2. Nozzles installed on the perimeter of the chamber to spray salt water
3. A pump that feeds the salt water into the tubing system
4. Infrared light casing containing two 250W infrared bulbs that can generate heat and dry the specimen.
5. Ultra Violet (UV) light casing containing to Philips T8 15W tubes that radiates UVC rays in the range of 250nm wavelength.
6. An inclined rack to hold the steel coupons that had the inclination slope (15^{o} to 30^{o}) according the recommendation from ASTM – B117
7. Timer switches to control the cycles of the actions of UV light, heat, and salt spray
8. Temperature and humidity meter

The proposed test cycle was customized to have appropriately harsh environment to achieve accelerated corrosion and deterioration of coating surface and steel. It includes 12 hours of freezing, 4 hours UVC radiation + infrared heating, 8 hours of saltwater spray. The lowest temperature during freezing was -23°C (-10°F); while the infrared induced temperature on black surface probe was up to 60°C. It is believed that the accelerate corrosion testing environment can better simulate field condition than the pure dry/wet testing cycle by submerging the specimen into salt water.

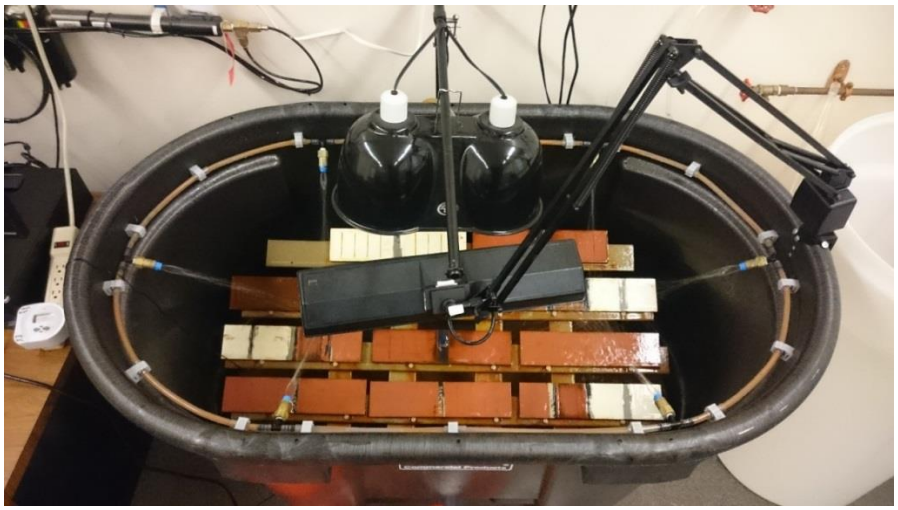

Figure 6 Customized corrosion chamber with coating specimens

The steel coupons that were used in the accelerated corrosion test were chosen to have the dimension of 12×4×0.5 inches. The coating thickness was measured using PosiTest DFT coating thickness gauge. The adhesion strength of coating was evaluated according to ASTM-D7234. The PosiTest AT-M Manual Adhesion Tester by Deflesko was used to perform adhesion strength test, as shown in Figure 7.

Figure 7 Manual adhesion tester and dolly

4.2 Testing Results of Hybrid Coating System

The first batch of hybrid coating system includes three types of coating samples. The first one was three-layer coating with two inorganic coating layers with one nano-film layer (proprietary product) in the middle. The second and third ones were inorganic coating with organic coatings on top, which were hi-solids polyurethane (B65W 311gloss surface and B65W 351 semi-gloss surface) purchased from Sherwin Williams. The thickness range of coatings was around 160-180 μm;

The coated steel plates were placed in the accelerated corrosion test chamber for 30 days. After that, the performance of coating was examined through visual observation and interface bonding strength. The testing results of pull-off strength and failure status are show in Table 1. Figure 8 illustrates the failure patterns at interface after pull-off tests for different coating samples, respectively, before and after accelerated corrosion test. The changes of pull-off strength after 30-day cycles were found not significant. The failure patterns at the interface indicated that no corrosion happened at the interface between coating and steel plate.

Table 1 Summary of Pull-off Strengths and Interface Failure Patterns (1st batch)

Corrosion System	Pull-off Strength (MPa) and Failure Pattern*								
	Before Corrosion Cycle					After One Month of Corrosion Cycle			
	A	B	C	D	E	A	B	C	D
3 - Layer Inorganic	9.61	6.28	8.06	7.07	4.14	6.59	5.18	3.65	5.06
	CF	CF	CF	CF	CF	CF	CF	CF	CF
Organic on top - Gloss	13.33	10.27	12.65	13.38	7.65	16.13	18.29	/	/
	AF-GD	AF-CS	AF-GD	AF-GD	AF-CS	AF-GC	AF-GC	/	/
Organic on top - Semi Gloss	17.74	15.08	12.52	12.65	13.63	17.27	15.07	/	/
	CF	CF	CF	AF-GD	CF	CF	CF	/	/

*CF: Cohesive failure in the coating; AF-CS: Adhesive failure (coating-steel)
AF-GD: Adhesive failure (glue-dolly); AF-GC: Adhesive failure (glue-coating)

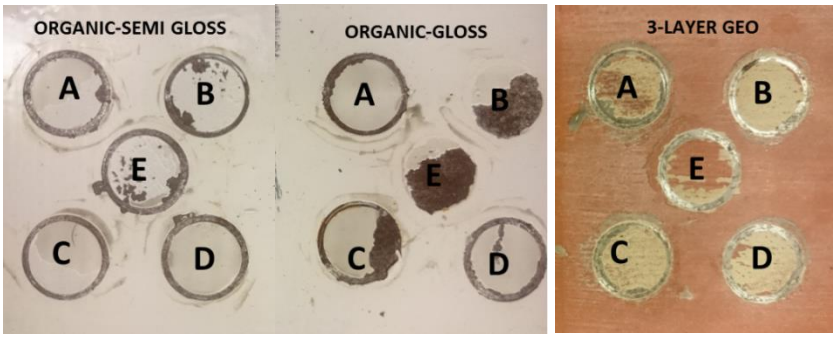

(a)

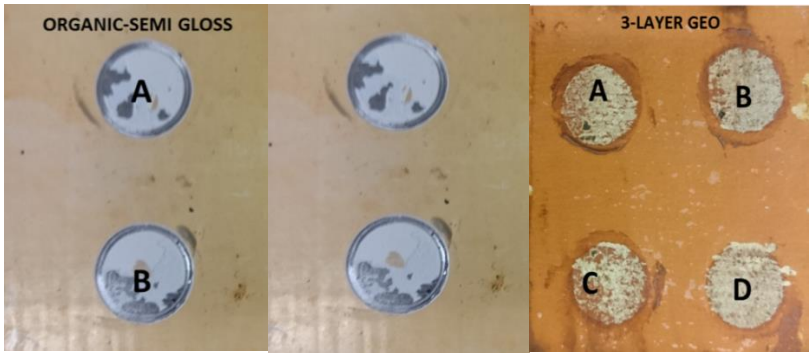

(b)

Figure 8 Failure patterns at interface after pull-off test: (a) before; and (b) after corrosion test

The second batch of hybrid coating system was prepared with three different coating combinations. The first one was inorganic coating with 3M sol-gel on top (150 μm). The second and third ones were inorganic coating topped with nano-film with two different thicknesses (150 μm and 210 μm). To prevent rust developed at the rare steel surface, the back sides of steel plates were coated with organic coating.

The summary of pull-off strength results before and after 30-dayand 60-day corrosion cycles is shown in Table 2. It was found that the pull-off strength increased after 30-day corrosion cycle, which was probably due to the continuous curing effect of coating. Figure 9 shows the interface failure patterns after pull-off test. It was found that the sample with 3M sol-gel performed well after 30-day cycles, but appeared with powdered surface after 60-day cycles. The geopolymer coatings with nanofilm performed well after 60-day cycles, although the pull-off strength decreased for one inorganic coating system. This also indicates that no corrosion happened to reduce the pull-off strength. The failure patterns at the interface indicated that no corrosion happened at the interface between coating and steel plate.

Table 2Summary of Pull-off Strengths and Interface Failure Patterns (2nd batch)

Inorganic Coating System	Pull Off Strength (MPa) and Failure Pattern*								
	Before corrosion cycle			After 30-day corrosion cycles			After 60-day corrosion cycles		
	A	B	C	A	B	C	A	B	C
3M Sol-Gel on top	3.73	4.26	4.17	9.01	8.13	10.92	N/A (due to powder surface)		
	CF	CF	CF	CF	CF	CF			
Nano-film on top (thin)	9.75	9.04	8.8	17.85	15	15.36	16.47	14	8.9
	NA	NA	NA	AF-GC	AF-GC	CF	AF-GC	AF-GC	AF-GC
Nano-film on top (thick)	4.74	4.46	4.15	16.47	13.85	13.99	8.56	7.32	7.29
	CF	CF	CF	AF-GC	AF-GC	AF-GC	AF-CS	AF-CS	AF-CS

*CF: Cohesive failure in the coating; AF-CS: Adhesive failure (coating-steel)
AF-GD: Adhesive failure (glue-dolly); AF-GC: Adhesive failure (glue-coating)

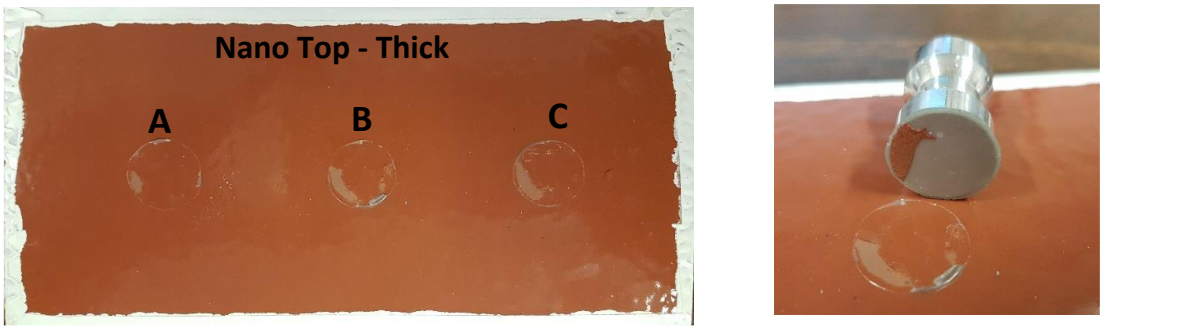

(a)

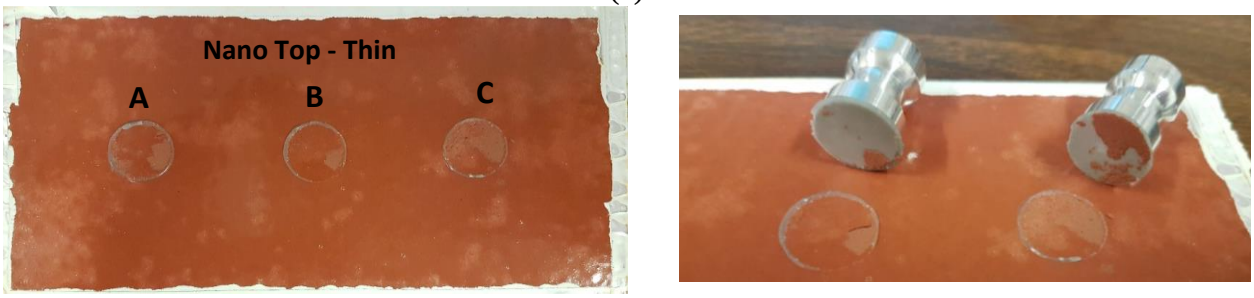

(b)

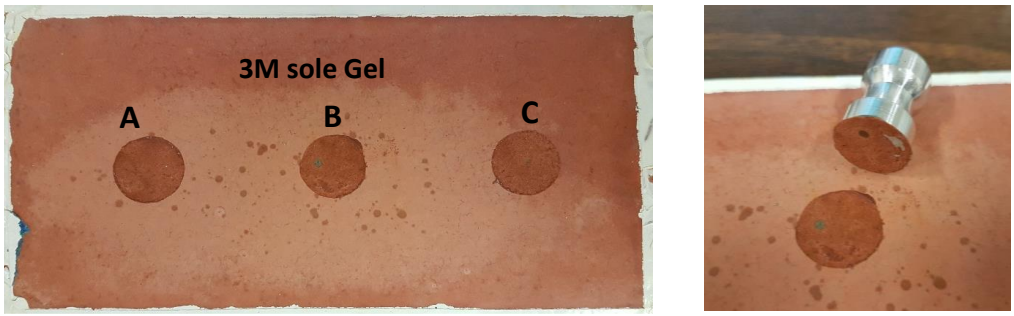

(c)

Figure 9Interface Failure Patterns of Different Coating Systems: (a) 3M sol-gel on top; (b) nano-film on top (thin); and (c) nano-film on top (thick)

4.3 Testing Results of Nano-Modified Coating

The first batch of nano-modified coating systems includes three nano-additives mixed with inorganic coating. Nano-additives were diluted in water with 20% iron oxide, 30% titanium oxide, and 30% silica in weight. The water amount from the solutions of nano-additives was accounted so that the total water content in the mix remained unchanged. In other words, the total water content in the nano-modified coating was kept the same as the one in the original coating formulation. The nano-additive was added at 1% of the coating mixture in weight.

Two coated specimens for each type of nano-additive and two control specimens were prepared, totally eight specimens. Surface preparation before coating application was performed. A decontamination cleaning foam was used to clean the grease oil from steel plates. Acetone could also be used to clean the contaminants off the steel surface. The steel plates were grit blasted or sand blasted prior to coating application.

Foam brushes were used to coat the steel specimens. After samples were cured, the finished coatings showed rough surfaces due to foam brush passes on the coated surface (Figure 10). As a result, pull-off test was not successfully performed on these sets of specimens. The observations of surface texture of the specimens showed that silica-added specimen had better finish with the least porous and glossier surface.

The coated plate specimens were placed in the accelerated corrosion chamber. The appearance of steel plates after 30-daycorrosion cycles is shown in Figure 11. The observation of specimens after the accelerated corrosion test concluded the following remarks:

1. It was clear that control specimen developed the signs of blistering earlier than other specimens. This was followed by the specimen added with iron oxide, the specimen added with titanium oxide, and the specimen added with silica.
2. In general, the control specimen and iron oxide added specimen were more severely affected by corrosion than the specimen added with titanium oxide or silica.
3. Foam brush left groove-like pattern on the surface of the specimens, which caused concentration of corrosion within these grooves.

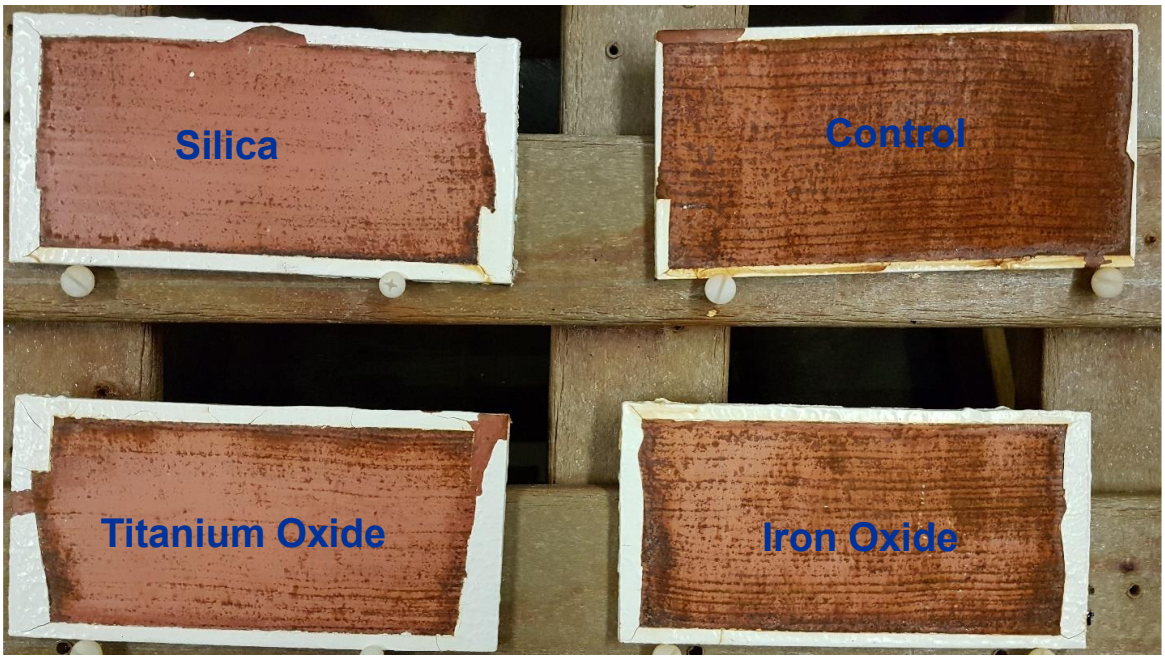

Figure10Coating appearances after30-dayin corrosion chamber
(From top left to bottom right, the nano-modifier was silica, control, titanium oxide, and iron oxide, respectively)

Microscopic image observation was conducted for all the coating specimens before and after corrosion cycles, as shown in Figure 11 and 12. Figure 11 showed there was no crack development in the coating before corrosion cycles. Figure 12 showed that rust developed within micro-cracks. This was probably because the freezing-thaw cycles caused thermal stress concentration in the coating layer. Comparatively, the coating specimen with nano-silica additive showed the few amount of micro cracks.

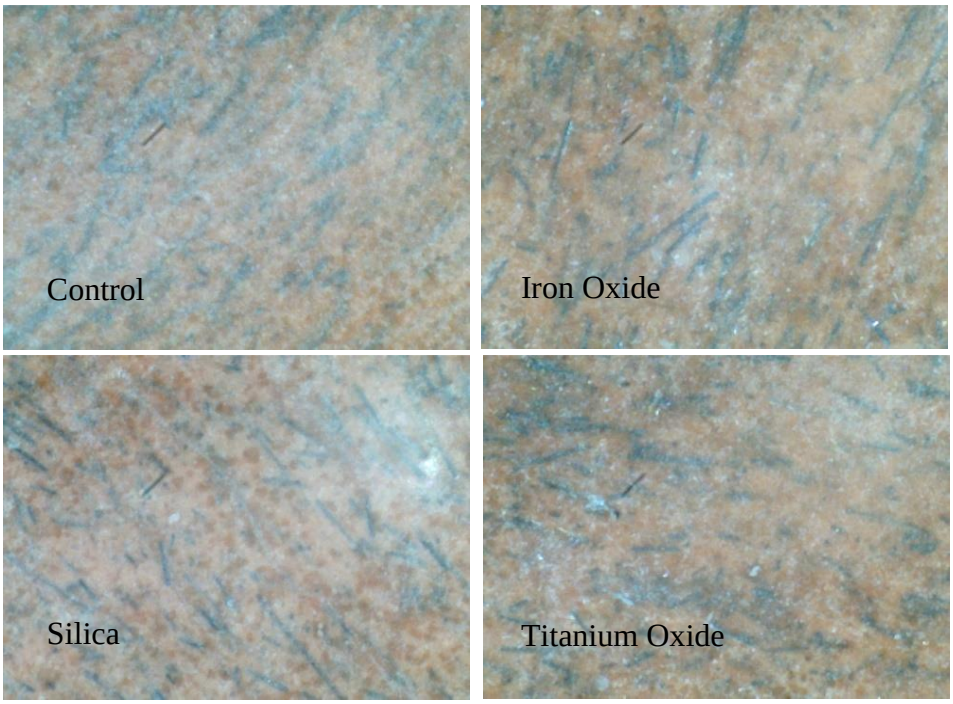

Figure 11 Macroscopic images of coatings before corrosion cycles

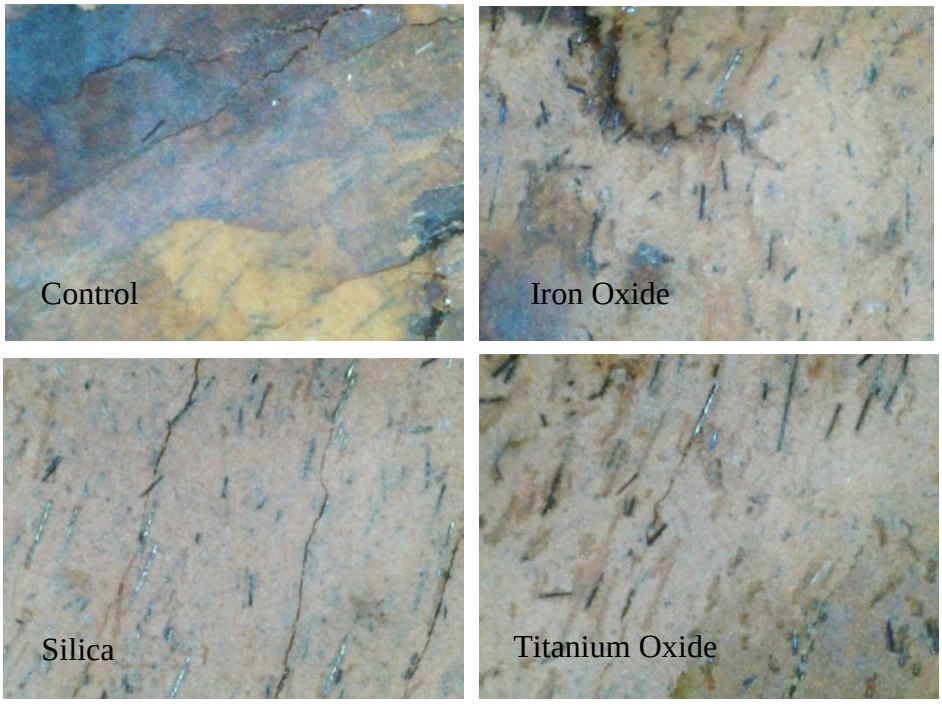

Figure 12Macroscopic images of coatings after corrosion cycles

To achieve uniformly coated surface, steel plates were coated using 1.4-mm nozzle tip high volume low pressure (HVLP) spray gun, as shown in Figure 13. The original water content in the coating mixture proved to be incompatible with this spray gun and coating could not be properly sprayed or sprayed at all. This was contributed by relatively higher viscosity and lower surface tension of the coating, which makes flow of coating difficult. Although the larger nozzle spray gun was able to spray original coating mixture, the results were found far from satisfactory. Because of the thick mixture, coating would be spattered in droplets on the surface and could not achieve smooth finish. Frequent clogging of gun nozzle also happened. To solve this problem, the water content was increased from 6.25% to 9.1% of coating mixture, which enables the HVLP spray gun to spray coating mixture.

Figure 13 HVLP spray gun for coating spray

The second batch of nano-modified coating system includes inorganic coatings modified with silica (SiO2), titanium-dioxide (TiO2), and graphene oxide. The prepared sample details are listed in Table 3. All samples were treated by organic coating at the back and sides of steel plates before accelerated corrosion test. The appearances of coating samples were shown in Figure 14.

Table 3 Summary of Nano-Modified Coating Samples

Additives	**Contents**
TiO_2 powder	1%, 3%, 5%
SiO_2 powder	1%, 3%, 5%
Graphene oxide	1%, 3%, 5%

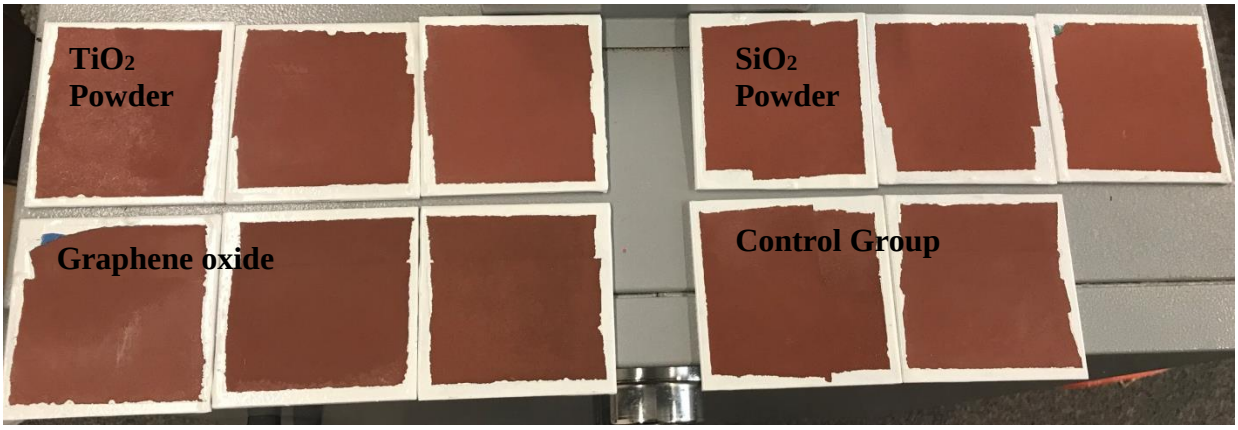

Figure 14 Coating samples with different nano-additives before testing

The appearances of coating samples after 30-daycorrosion cycles are shown in the Figure 15-17, respectively, for the coatings added with titanium oxide, silica, and graphene oxide. In these figures, the pictures from left to right were observed with the increase of testing time and the changes of coating appearance were observed.

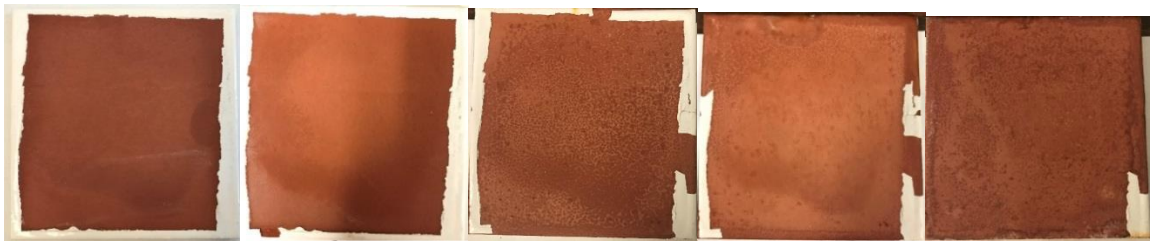
(a)

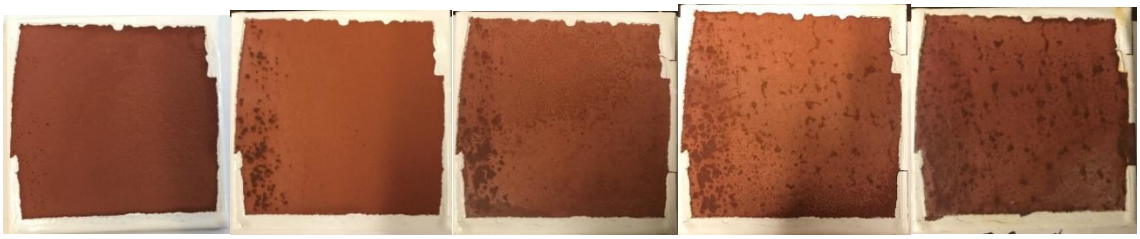
(b)

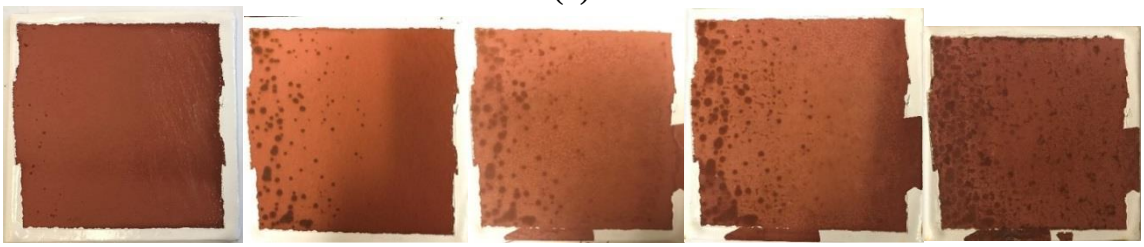
(c)

Figure 15 Appearances of coating samples with (a) 1%; (b) 3%; and (c) 5% titanium oxide after 30-day corrosion cycles

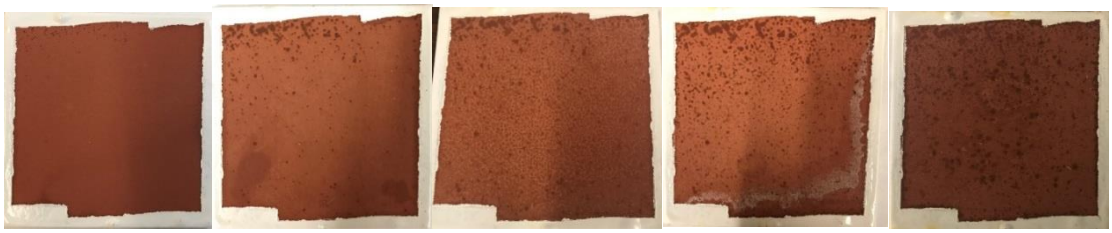

(a)

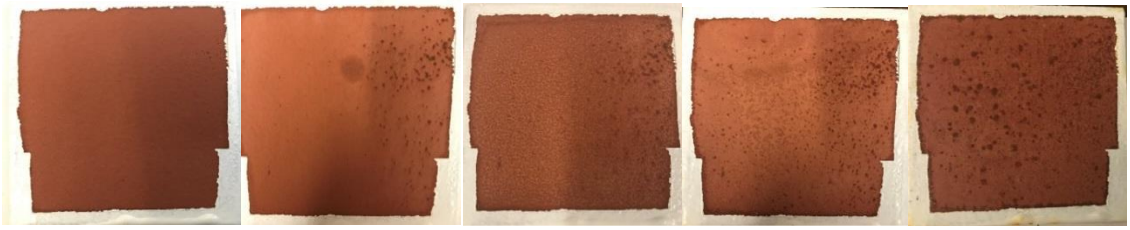

(b)

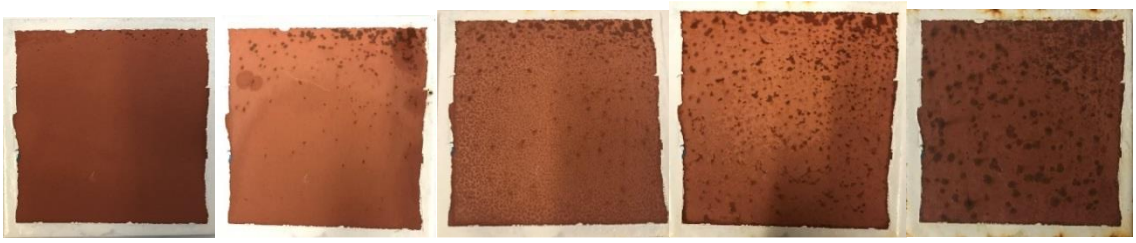

(c)

Figure 16 Appearances of coating samples with (a) 1%; (b) 3%; and (c) 5% silica after 30-day corrosion cycles

(a)

(b)

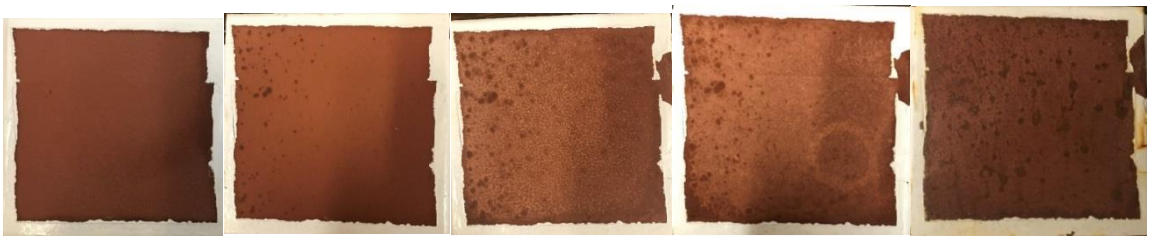

(c)

Figure 17 Appearances of coating samples with (a) 1%; (b) 3%; and (c) 5% graphene oxide after 30-day corrosion cycles

Table 4 lists the coating thickness for different samples. Relating the coating thickness with the observed coating appearance after accelerated corrosion testing, it was noted that thin coating layer had relatively more black dots after corrosion test, and as for all samples, because of the uneven thickness, the black dots were usually generated from thin area, e.g. Ti-3%, Ti-5%, Graphene-1%, etc. samples.

The pull-off strengths of all coating samples after 30-day corrosion cycles were measured, as shown in Table 5. Among three different nano-additives, SiO2 resulted in the slightly greater bonding strength between coating and steel plate.

Table 4 Summary of Thickness for Different Coating Samples

Samples	Thickness, um								
	TiO_2			Graphene oxide			SiO_2		
	1%	3%	5%	1%	3%	5%	1%	3%	5%
Average	245	192.5	194	168	348	253	168	205	211.5
Standard deviation	26	28	35.5	24	38	40	11	33	33

Table 5 Pull-Off Strength Test Results (after 30-day corrosion test)

Samples	Bonding strength (MPa)			Average(MPa)
TiO_2 1%	2.95	3.68	4.19	3.61
TiO_2 3%	3.95	2.84	3.58	3.46
TiO_2 5%	3.47	3.68	-	3.58
SiO_2 1%	4.55	4.52	-	4.54
SiO_2 3%	3.36	4.16	3.95	3.82
SiO_2 5%	3.7	3.98	-	3.84
Graphene oxide 1%	4.51	4.37	4.05	4.31
Graphene oxide 3%	3.11	3	3.39	3.17
Graphene oxide 5%	4.01	3.54	3.37	3.64

Chapter 5 Shear Strength Testing of Coating and Composite Repair

5.1 Shear Strength between CFRP and Steel

The inorganic coating was proposed to be used as barrier between carbon fiber reinforced polymer (CFRP) and pipeline steel to prevent carbon induced corrosion of steel while benefiting from light weight and high strength of carbon fiber. However, it is important that the bonding strength between pipeline steel and CFRP is high enough to carry the shear stress induced in the composite repair. Therefore, lap shear tests were conducted to measure the shear bonding strength between CFRP and steel with and without coating. For the overwrap composite repair of pipeline, the ASME PCC-2 standard requires the adhesive bond to be stronger than the lap-shear strength between the laminate and the metal substrates and with minimum shear strength of 580 psi (4 MPa).

The following standards and literature are reviewed. Through the examination of existing ASTM standards and other related literature, three candidate test setups were selected for comparison.

- ASTM D1002 Standard Test Method for Apparent Shear Strength of Single-Lap-Joint Adhesively Bonded Metal Specimens by Tension Loading (Metal-to-Metal)
- ASTM D3165 Standard Test Method for Strength Properties of Adhesives in Shear by Tension Loading of Single-Lap-Joint Laminated Assemblies
- ASTM D3528 Standard Test Method for Strength Properties of Double Lap Shear Adhesive Joints by Tension Loading
- Schnerch, David, et al. "Strengthening Steel Structures and Bridges with High-Modulus Carbon Fiber-Reinforced Polymers Resin Selection and Scaled Monopole Behavior." Transportation Research Record: Journal of the Transportation Research Board 1892 (2004): 237-245.
- Fawzia, Sabrina, Riadh Al-Mahaidi, and Xiao-Ling Zhao. "Experimental and finite element analysis of a double strap joint between steel plates and normal modulus CFRP." Composite structures 75.1 (2006): 156-162.
- Liu, Hong bo, and et al. "Prediction of fatigue life for CFRP-strengthened steel plates." Thin-Walled Structures 47.10 (2009): 1069-1077.

The test setup is based on the one recommended by ASTM D1002-10, which was modified to include CFRP laminate as the mediator part overlapped with two steel sheets. The overlap length (bond length) on one metal sheet was held to be constant (a); while the bond length (b) changed on the other steel sheet. This was used to investigate bond failure behavior with change of bond length on the coated and uncoated steel sheet samples. A displacement control tensile loading with the rate of 1.27mm/min was applied to the specimen till failure occurs, which was adopted from ASTM D1002. Figure 2 shows the test setup and the picture of lap shear test.

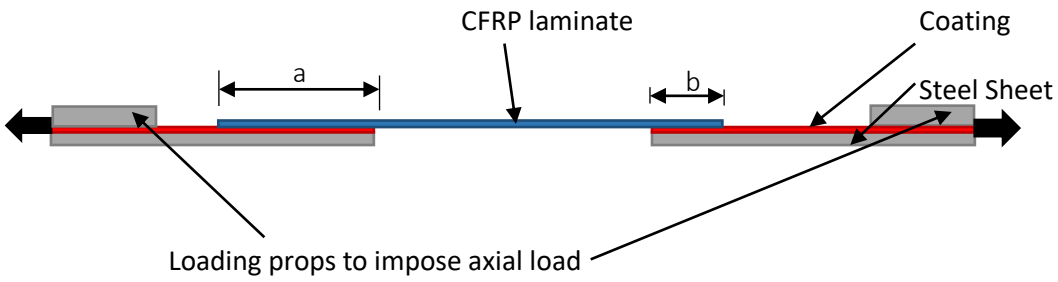

(a)

(b)

Figure 18 Illustration of (a) test setup and (b) picture for lap shear test

Figure 19 shows the measured tensile force and stress curve for the steel plates with CFRP (without coating) obtained from the lap shear test. The specimen was prepared to have an overlap length of 55mm at one end and 20mm at the other end. It was found that the ultimate shear strength was at the range of 12-14Mpa based on the assumption of uniform shear stress at the interface, which is consistent with the data reported in the literature (Schnerch et al. 2004) and by DowAska data sheet. However, the failure displacement may be a little bit high. There may be some slippage between the alignment piece at the ends of plates and the steel sheet and/or between the steel sheet and MTS grips.

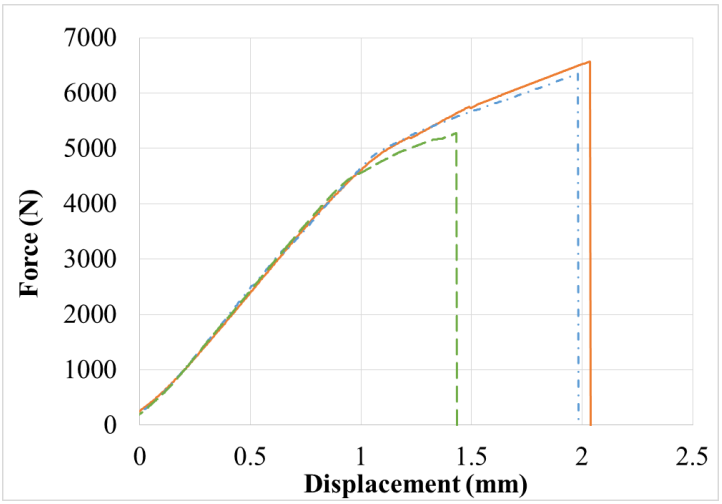

(a)

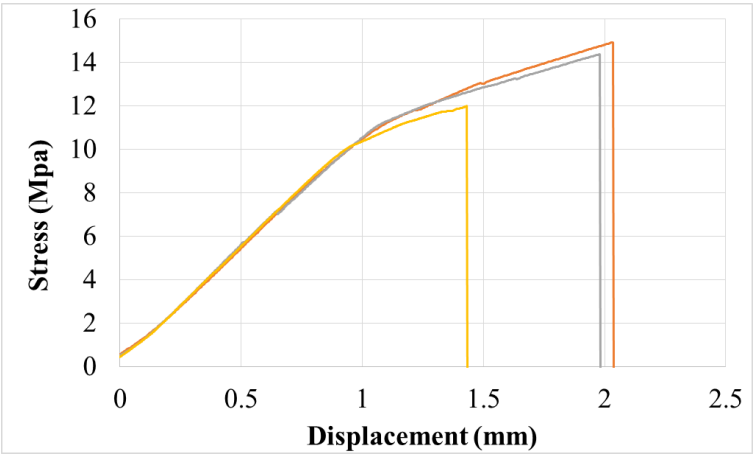

(b)

Figure 19 Measured (a) force; and (b) stress from lap shear test

5.2 Shear Strength between Coating and CFRP

A medium weight unidirectional carbon fabric (DowAksa CFU20T) was used to fabricate Carbon Fabric Reinforced Polymer (CFRP). The tensile modulus of CFRP was 16.2Msi (111.7GPa) for medium weight carbon fabric based on the data provide by manufacturer. The DowAksa CarbonBond 300-HT two-part saturant resin was used to impregnate carbon fabric.

The carbon fabric was first cut to desirable dimensions. Saturant resin was prepared by mixing Part-A and Part-B components of CarbonBond 300-HT. The mixing ratio for Part-A and Part-B was 3.1:1 by weight or 2.75:1 by volume, respectively. The mix should reach homogenous sate and resemble uniform red color. The carbon fabric sheet was impregnated using a spoon or spatula on both sides. The recommended application temperature is recommended to be 20°C to 25°C. The higher temperatures may result in accelerated curing and shorten the pot life of the resin mix; while the lower temperatures will increase viscosity of the mix and affect impregnation of carbon fabric. The CFRP will gain peak strength after curing in room temperature for about two weeks.

This process can be expedited by curing the CFRP at high temperature (110°C or 220°F) for at least 2 hours after an initial 2 hours of curing at room temperature.

Three specimens were prepared for uncoated and coated steel sheets with CFRP laminates, respectively, as shown in Figure 20. The bonding length between CFRP and steel was 20 mm at both ends. Each of the steel sheets at two ends of the specimens was sand blasted prior to fabrication of specimen. The reason that 20-mm bond length was chosen as comparison basis was that the peeling stresses at edge of CFRP were less severe and the stress distribution along the bond is more uniform for the shorter bond length. In addition, it was found in finite element analysis that steel sheets would go into yielding phase if the bond lengths are longer than 20mm. Coatings on the steel sheets were performed using spray gun. The lap-shear tests were conducted using MTS machine with displacement control at displacement rate of 12.7 mm/min.

Figure 20 Lap-Shear specimens prepared: uncoated (left) and coated (right).

The load-displacement curves are shown in Figure 21. The calculated average failure stresses (bond strengths) are summarized in Table 6. It is noted that specimen Coated-20-1 was found to be defective due to fabrication quality and thus not tested. The results show that although the shear bong strength decreased after adding the coating, the shear strength is still greater the 4-MPa requirement for over-wrap composite repair (ASME PCC-2 standard).

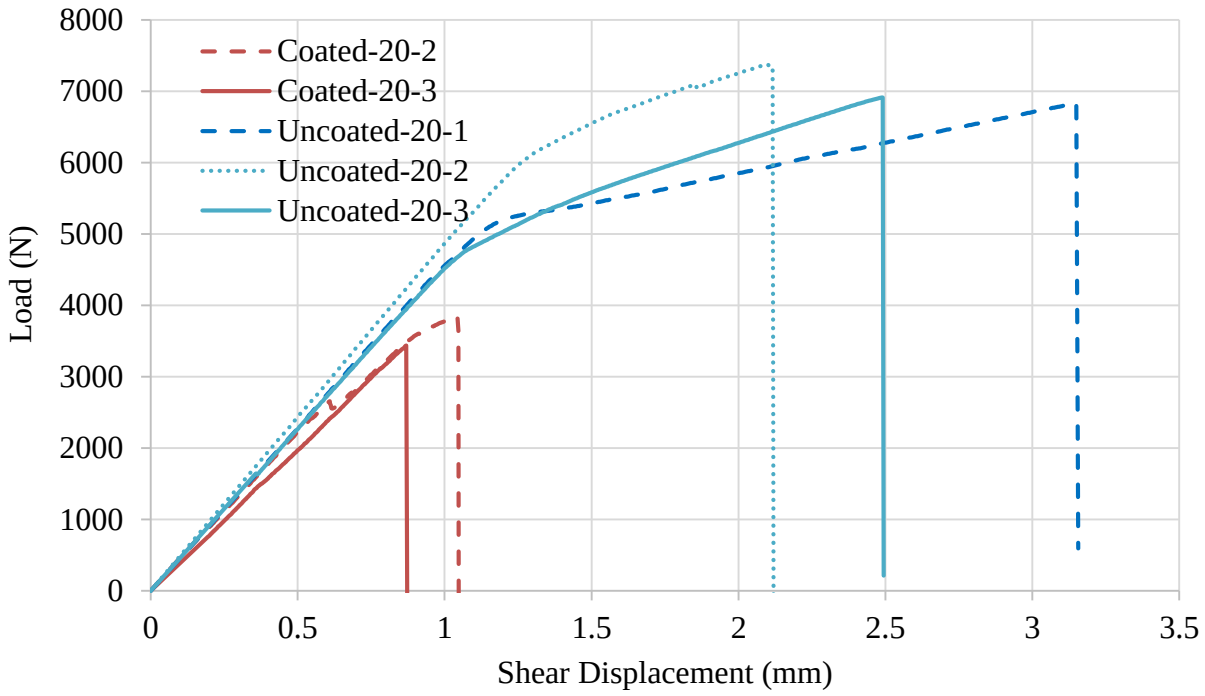

Figure 20 Load-displacement curves for lap-shear tests

Table 6 Ultimate Loads and Shear Bond Strengths for Coated and Uncoated Specimens

Specimen	Ultimate load (N)	ShearBond strength(MPa)
Coated-20-2	3650	9.1
Coated-20-3	3440	8.6
Uncoated-20-1	6836	17.1
Uncoated-20-2	7336	18.3
Uncoated-20-1	6913	17.3

The appearances of specimens after failure are shown in Figure 21. The failure patterns were consistent showing the interface debonding between steel plate and coating.

Figure 21 Specimens after failure (from left to right): Coated-20-2, Coated-20-3, Uncoated-20-1, Uncoated-20-2, Uncoated-20-3.

5.3 Pull-off Strength between Coating and Resin used in CFRP

Two specimens were coated with inorganic coating using spray gun and cured in the oven at 80°C (175°F) for 72 hours. DowAksaCarbonBond300H saturant resin used in CFRP was applied on top of the cured coating samples. Thickness measurements were repeated on top of the coating and the average thicknesses were 144 and 152μm on two specimens, respectively. Pull-off test was conducted on coated specimens to measure the bonding strength between saturant resin and inorganic coating. Table 7lists the measurement data of pull-off strength and the average value was found being around 5MPa. Figure 22 shows the post-failure appearances of specimens after pull-off test. It can be seen clearly that the failure occurs at the interface between resin and coating.

Table 7 Pull-Off Strength of Saturant Resin on Coated Specimen

Sample	Pull Off Strength (MPa)			
	1	2	3	Average
1	5.4	5.1	NA	5.25
2	5.2	4.6	5.2	5.03

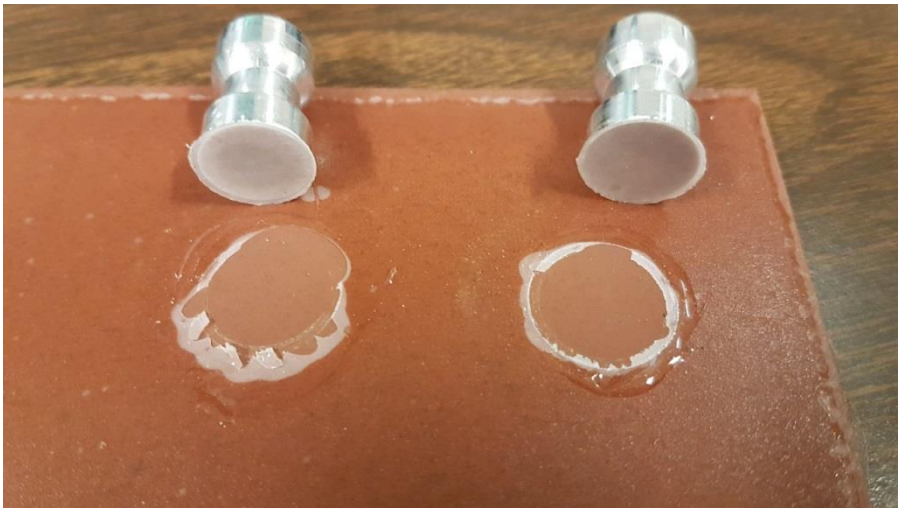

Figure 22Pull off strength performed on coated steel specimen topped with DowAksa CarbonBond 300H Saturant Resin

5.4 Shear Strength between Nano-modified Coating and CFRP

Various nano-modified coatings were tested with CFRP for shear bonging strength. The bond length on the coated steel sheet end was selected to be 30mm. The bond length at the opposite end on uncoated steel sheet was selected to be 50mm. DowAksa Carbon300H resin was used to impregnate the carbon fabric pieces for specimen fabrication. The specimens were cured for 10 days in room temperature after they were are in the oven at 60°C for 48 hours. Figure 23 shows the samples prepared for lap shear test. A total of 22 specimens were tested. The lap shear tests were conducted using an MTS machine with 12.7mm/min displacement control loading.

.

Figure 23 Samples prepared for lap shear test

Figure 24 shows the appearances of post-failure specimens after lap shear test. It was observed that almost all failures occurred at interface between coating and steel, which is consistent with unmodified coating. This also indicated good adhesion of resin with inorganic coating.

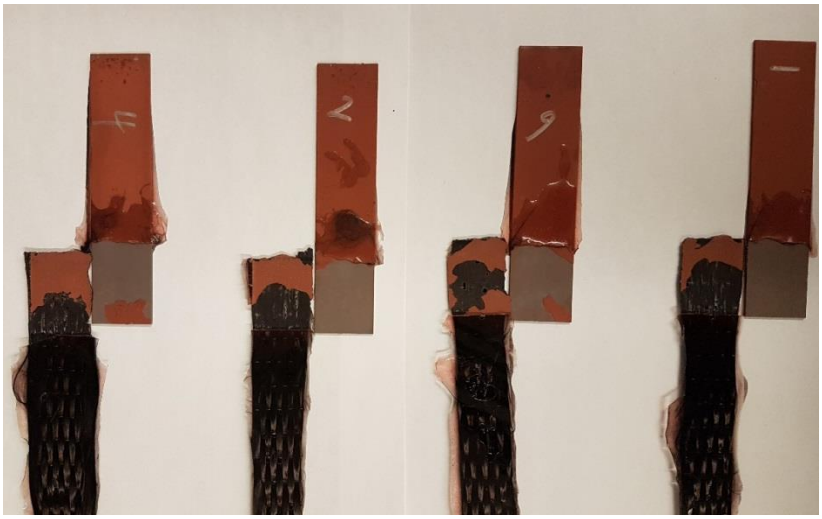

Figure 24Specimens after failure at the end of coated steel sheet

Table 8-10 shows the shear bond strength measured for three groups of nano-additives. The minimum average bond strength of 4.4MPa was observed in nano-modified samples; while the maximum average bond strength of 11.7MPa was observed. The coating modified with SiO_2 performed the best in general. The second best performance was observed for the coating modified with TiO2 powder. It was observed that the average bond strength increased with increase of the percentage of SiO_2 and TiO_2. However, this increasing trend of bonding strength was not observed for graphene oxide.

Table 8 Bond Strengths Measurements for Samples with SiO_2

SiO2 Nano Compositions	Shear Bond Strength	Average Strength
1% SiO2 Powder - S11	8.7	7.25
1% SiO2 Powder - S6	5.8	
3% SiO2 Powder - S1	7.0	7.7
3% SiO2 Powder - S2	8.4	
5% SiO2 Powder - S5	9.4	10.5
5% SiO2 Powder - S10	11.7	

Table 9 Bond Strengths Measurements for Samples with TiO_2

TiO2 Nano Compositions	Shear Bond Strength	Average Strength
1% Ti Powder - S15	3.7	4.0
1% Ti Powder - S16	4.4	
3% Ti Powder - S8	6.4	6.4
3% Ti Powder - S14	6.5	
5% Ti Powder - S3	7.7	6.7
5% Ti Powder - S20	5.6	

Table 10 Bond Strengths Measurements for Samples with graphene oxide

Graphene-Oxide Nano Compositions	Shear Bond Strength	Average Strength
1% Graphene Oxide - S12	5.0	5.8
1% Graphene Oxide - S21	6.6	
3% Graphene Oxide - S4	5.5	5.5
3% Graphene Oxide (wide) - S22	6.5	
5% Graphene Oxide - S9	5.5	5.7
5% Graphene Oxide - S17	5.8	

Chapter 6 Analytical Study of Composite Repair of Pipeline

6.1 Development of FE Model

The primary objective of analytical study is to evaluate mechanical behavior of the defected pipeline repaired with carbon fiber reinforced polymer (CFRP) using finite element (FE) analysis. Two different repair methods namely wrap repair and patch repair, were considered. The mechanical behavior of the pipeline with composite repair system was analyzed in terms of burst pressure and maximum allowable operating pressure (MAOP). The presented model was validated with existing experimental data of burst pressure. Sensitivity analysis was conducted to analyze various parameters affecting the design of composite repair system, including patch size and thickness, infill material, adhesive layer, and interface bonding condition.

The 3D FE model was developed with commercial FE software ABAQUS. The dimension of the pipeline segment model is shown in Figure 25(a). The outer diameter and length of the steel pipe were 168.3 mm and 1520 mm, respectively. The thickness of steel wall was 7.11 mm. In the symmetrical model, the half-length of the steel pipe was 760 mm. Different sized defects in the steel pipe wall were simulated to represent metal loss due to external corrosion, as shown in Figure 25(b). The defect depth in the radial direction and the length in the axial direction were assumed 3.56 mm and 152.4 mm for all defects. In the hoop direction, the defect length was either 152.4 mm or equal to the perimeter of the pipe (full circle).

In the symmetrical model, the half-length of the defect in the axial direction was 76.2 mm. Two different repair strategies were evaluated in this study. One is wrap repair, and the other is patch repair. For the wrap repair as shown in Figure 25(c), the defect in the steel pipe wall was filled with repair material (adhesive putty), and then CFRP wraps were applied along the hoop to cover the defect. While for the patch repair as shown in Figure 25(d), the CFRP was not applied along the hoop, but was patched over the defect with a specific length in the hoop direction. It should be noted that the patch repair was only applied to the defect with 152.4-mm length in the hoop direction since the area of composite patches should be larger than the defect. Different sized patches were used in the analysis.

In the FE model, the cap of the pipe was meshed with ten-node quadratic tetrahedron elements and free meshing technique. The other sections including the pipe wall, infill material, and the CFRP were meshed with eight-node brick elements and structured meshing technique. The meshes were refined around the defect area along the axial direction. In the radial direction, the pipe wall and infill material were divided into 16 and 10 layer of elements, respectively. The layers of elements in the radial direction for CFRP were determined depending on the thickness of CFRP. The CFRP layer was divided into different numbers of sublayers depending on the layer thickness.

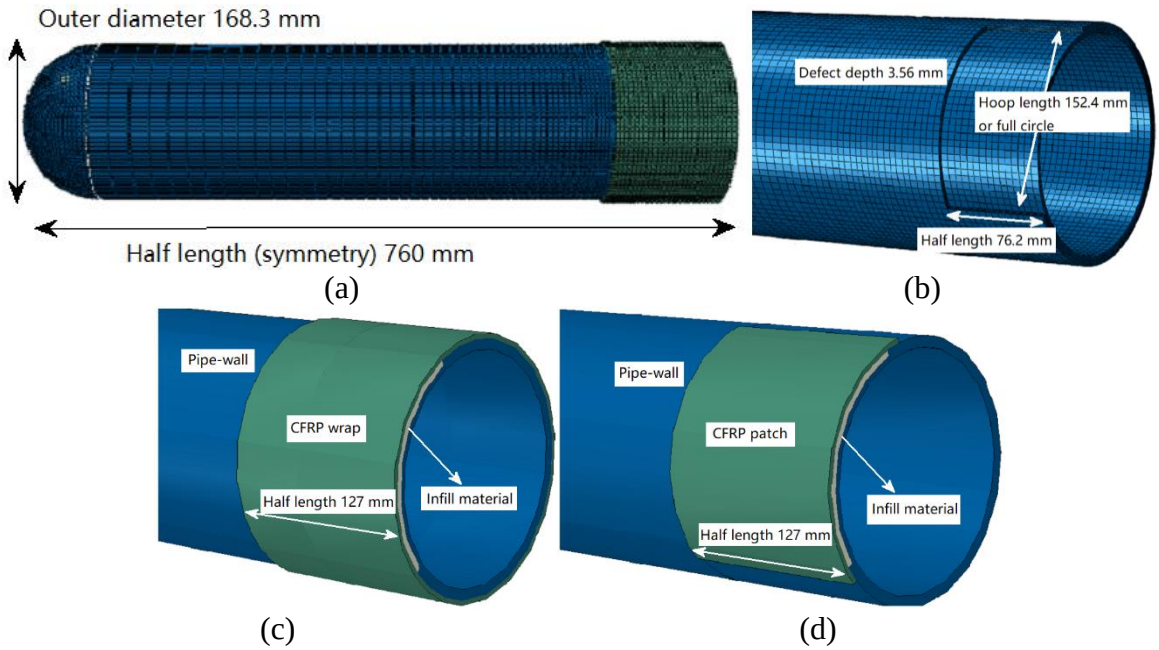

Figure 25 Model dimension: (a) whole model; (b) defect; (c) wrap repair; and (d) patch repair

6.2 Material properties

In this study, the ASTM A106 Grade B steel was used for the pipe wall. The repair material used was the thickened epoxy. Two different thicknesses were considered for CFRP layer: 3.1mm for six layers of CRFP and 6.2mm for 12 layers of CFRP. The material properties used in the FE model are shown in Table 11, which are based on an experimental study conducted in the previous work (Duell et al. 2008).

6.3 Model validation

In order to validate the FE model in this study, the burst pressure calculated with the FE model was compared with the experimental data reported in the literature (Duell et al. 2008). In the validation, the CFRP wrap repair was used and the thickness of the CFRP was 3.1 mm. It is assumed that the pipe wall, infill material, and CFRP were full bonded and no slip was allowed at the interfaces between different materials. The internal pressure was increased from 40 MPa to 45 MPa at the interval of 0.1 MPa. The system was considered as burst failure when the von Mises equivalent stress in the steel reached the true ultimate tensile strength or when the maximum hoop stress in the CFRP exceeded its ultimate hoop strength.

The burst pressure predicted from the FE model was shown in Figure 26, together with the experimental and numerical data reported in the literature (Duell et al. 2008). The simulation results show that the hoop stress in the CFRP exceeded its ultimate hoop strength before the von Mises equivalent stress in the steel reached the true ultimate tensile strength. The relative difference between the predicted and experimental values was 0.69% for the pipe with 152.4 mm defect in the hoop direction, and 5.48% for the pipe with full circle defect in the hoop direction. This indicates that the accuracy of the developed FE model is acceptable.

Table 11 Material properties in FE model (Duell et al. 2008)

Material	Properties			
	Linear (below yield)		Nonlinear (above yield)	
Steel	Young's Modulus	207 GPa	Yield Stress (MPa)	Plastic Strain
			301	0.0000
			317	0.0029
			374	0.0138
			412	0.0207
	Poisson's Ratio	0.3	482	0.0386
			534	0.0575
			596	0.0862
			648	0.1222
Epoxy	Young's Modulus	1.74 GPa	Yield Stress	33 MPa
	Poisson's Ratio	0.45	Tangent Modulus	0.87 GPa
CFRP	Young's Modulus	E_1 5.5 GPa (radial)	Poisson's Ratio (assumed)	ν_{12} 0.1
		E_2 49 GPa (hoop)		ν_{13} 0.4
		E_3 23.4 GPa (axial)		ν_{23} 0.4
	Shear Modulus	G_{12} 29.6 GPa		
		G_{13} 0.69 GPa		
		G_{23} 0.69 GPa		
	Ultimate Hoop Strength	576 MPa		

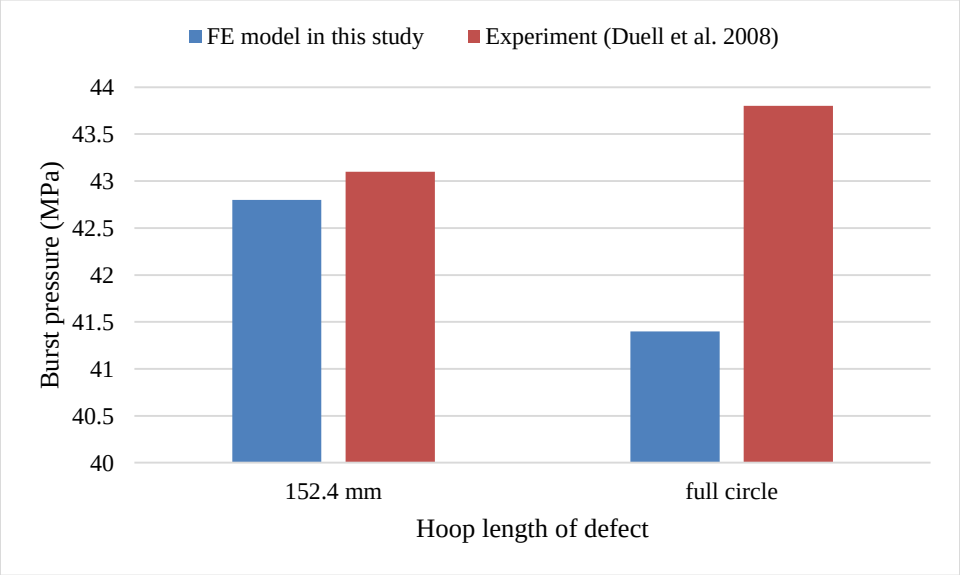

Figure 26 Validation of burst pressure obtained from simulation and experiment

6.4Effect of CFRP patch size

In most cases, the internal pressure of pipeline is much lower than the burst pressure of the undamaged pipeline. Therefore, in the following analysis, the maximum allowable operating pressure (MAOP) is used instead of burst pressure. In practice, the MAOP cannot exceed the lowest value among design pressure, test pressure, maximum operating pressure during five years preceding the applicable date of pipeline, and the maximum safe pressure determined by the operator (49 CFR 192.619). In this study, the design pressure was used to determine the MAOP, since the design pressure can be simply determined with Barlow's formula as shown in Eq. (1) (Motta et al. 2017). For the pipeline used in this study, the design pressure could be calculated as 18.25 MPa based on Equation (2).

$$\mathrm{P} = \frac{2St}{D} \times F \times E \times T \tag{2}$$

Where, P is design pressure; S is yield strength of steel; t is the nominal wall thickness of pipe; D is the outside diameter of pipe; F is design factor, equal to 0.72 for liquid pipeline and Class 1 gas pipeline; E is longitudinal joint factor; and T is temperature factor.

The effect of CFRP thickness and size on mechanical behavior of composite repair system under the MAOP was analyzed. The CFRP patches with two different thicknesses (3.1 mm and 6.2 mm) in the radial direction were used. The CFRP length in the hoop direction ranged from 161 mm (slightly larger than the defect) to 264 mm (half of pipe perimeter). In addition to patch repair with different sizes, one case of CFRP wrap repair was calculated for comparison. The maximum von Mises stress in the pipe wall and the maximum hoop stress in the CFRP were calculated under the MAOP.

Figure 27 shows the maximum von Mises stress in the pipe wall for different cases. As shown in Fig.3, the effect of CFRP size on the maximum von Mises stress was negligible for the 3.1-mm CFRP patch. While for the 6.2-mm CFRP patch, the maximum von Mises stress in the pipe wall generally decreased with the increase of patch size. When the length of 6.2-mm patch is larger than 235 mm in the hoop direction, the von Mises stress in the steel pipe repaired with patch repair could be smaller than that repaired with wrap. This indicates it is feasible to use patch repair instead of wrap repair when the CFRP layer is relatively thick. Moreover, under the MAOP, the 6.2-mm CFRP patches could provide reliable reinforcement since the maximum von Mises stress in the pipe-wall was controlled below the yield strength. However, for the 3.1-mm CFRP, the maximum von Mises stress in the pipe wall exceeded the yield strength for both patch repair and wrap repair, indicating that the CFRP need have certain thickness to be effective.

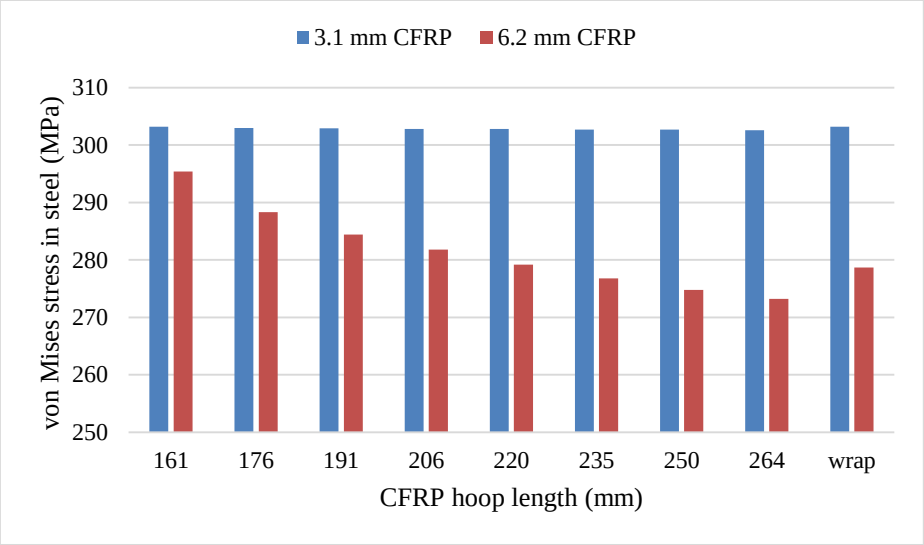

Figure 27 Maximum von Mises stress in the pipe-wall for patch sizes as compared to wrap repair

Figure 28 shows the calculated maximum hoop stresses in the CFRP for patch repair with different hoop lengths and wrap repair. As shown in Fig.4, the maximum hoop stress in the CFRP increased slightly with the increase of patch size in the hoop direction. This indicates that more stress could be transferred to CFRP when the patch size is larger. The hoop stress in the CFRP patch was slightly smaller than that in the CFRP wrap for the 3.1-mm CFRP; but very close to each other for the 6.2-mm CFRP. On the other hand, the hoop stress in the 3.1-mm CFRP was found much greater than the one in the 6.2-mm CFRP.

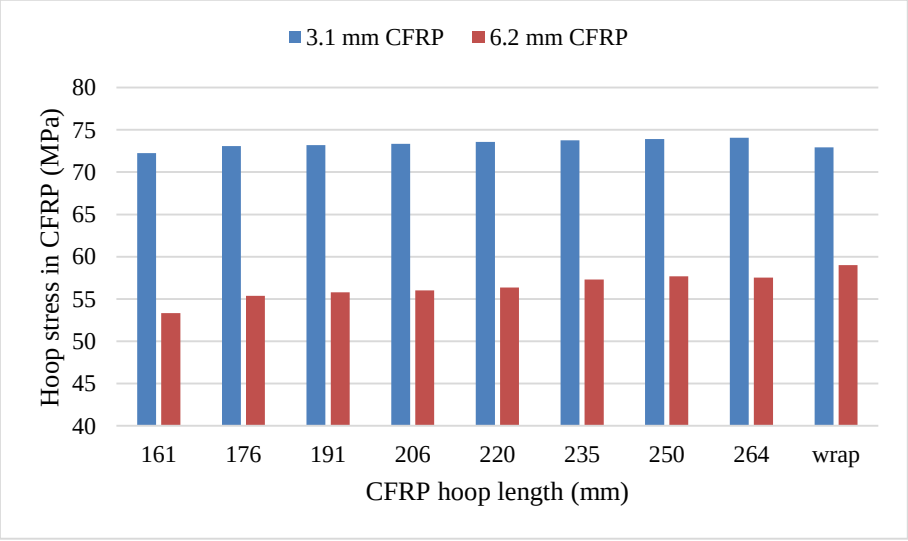

Figure 28 Calculated maximum hoop stresses in the pipe-wall for patch repair with different hoop lengths and wrap repair

6.5 Effect of modulus of infill material

In the composite repair system, the stress is mainly carried by the pipe wall and the CFRP. The infill material is usually polymer material with relatively lower elastic modulus, such as epoxy.

However, as an intermediate layer between pipe-wall and CFRP, the modulus of infill material could have effect on load transfer mechanism in the repair system. The developed inorganic composite can be as alternative binder material. The elastic modulus of the inorganic composite could range from 10GPa to 20GPa, depending on the chemical composition and polymerization process (Balaguru and Lee 2001). The effect of infill material modulus on mechanical behavior of composite repair system under the MAOP was analyzed. The CFRP with the thickness of 3.1 mm was not used in this section, since the pipe-wall may yield under the MAOP based on the previous analysis.

The maximum von Mises stress in the pipe wall, and the maximum hoop stress in the 6.2mm CFRP, for repair systems with different infill materials are shown in Figure 29. It can be seen that for any given CFRP size, the von Mises stress in the steel pipe repaired with 10GPa inorganic composite was greater than that repaired with 20GPa inorganic composite, but smaller than that repaired with epoxy. In other words, the von Mises stress in the steel pipe decreases for all patch sizes with the increase of elastic modulus of filling material. Similarly, the hoop stress in the CFRP decreases for all patch sizes with the increase of elastic modulus of filling material. This indicates the reinforcement of the CFRP repair system could be enhanced by using infill material with higher elastic modulus.

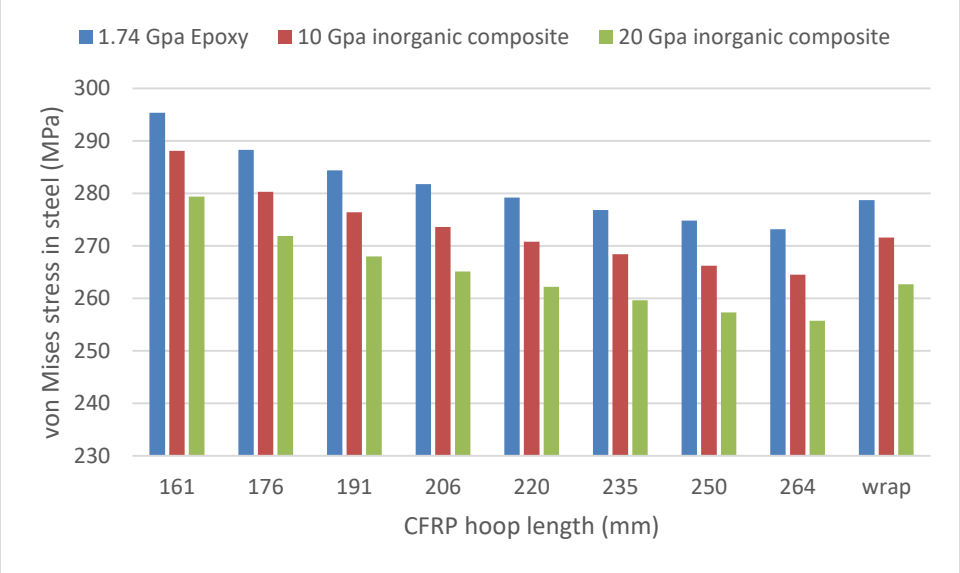

(a)

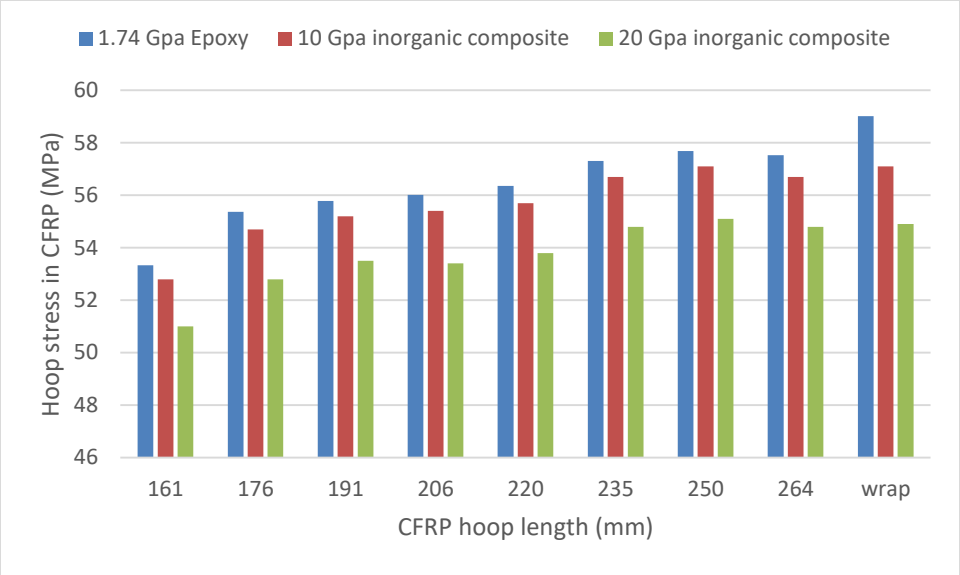

(b)

Figure 29 Effect of infill modulus on (a) von Mises stress in pipe and (b) hoop stress in CFRP

6.6 Effect of adhesive layer

In the previous FE models, the CFRP patches and wraps were assumed to be bonded directly with the infill material and the pipe wall with thin adhesive whose thickness could be ignored. In practice, the resin layer in the CRFP is thickened to prevent corrosion potential caused by the contact between steel pipe wall and carbon fiber (Tavakkolizadeh and Saadatmanesh 2001). This is equivalent to the case there is an extra adhesive layer between CFRP and pipe wall. In this section, the effect of adhesive layer modulus on mechanical behavior of the pipeline and composite repair system was investigated. The 6.2-mm CFRP were used to repair the pipe in patches and wrap. A 2-mm adhesive layer was simulated to bond the CFRP with the infill material and the pipe-wall. The epoxy was used as infill material. The adhesive material was assumed to be either epoxy putty with elastic modulus of 1.74 GPa or the inorganic composite with elastic modulus of 10 GPa.

Figure 30 shows the calculated maximum von Mises stress in the pipe wall under the MAOP at different scenarios of adhesive layer. It can be seen that with the 2-mm adhesive layer, the maximum von Mises stress in the pipe wall increased for all cases. An opposite trend was observed for the maximum hoop stress in the CFRP, as shown in Figure 31. After having 2-mm adhesive layer, the maximum hoop stress in the CFRP decreased for all cases. This indicates that with the addition of thin adhesive layer, the pipe wall bears more stress while the CFRP carries less stress. The main reason for this trend is that the modulus of adhesive layer is smaller than that of CFRP and steel pipe, so that the stress cannot be effectively transferred from steel pipe wall to CFRP. Therefore, the effect of using high-modulus (10-GPa) adhesive material was further investigated. The results in Figure 30 and Figure 31 show that the use of high-modulus adhesive material causes the reduction of von Mises stress in steel but the increase of hoop stress in CFRP. This indicates that the ability of stress transfer is stronger as the modulus of adhesive layer increases.

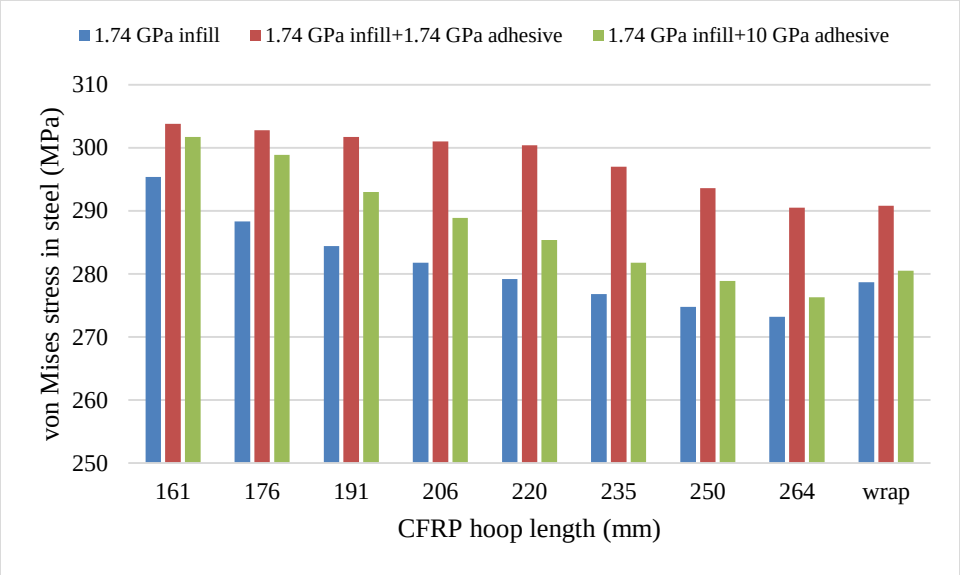

Figure 30 Effect of adhesive on von Mises stress in pipe with infill material of 1.74 GPa epoxy

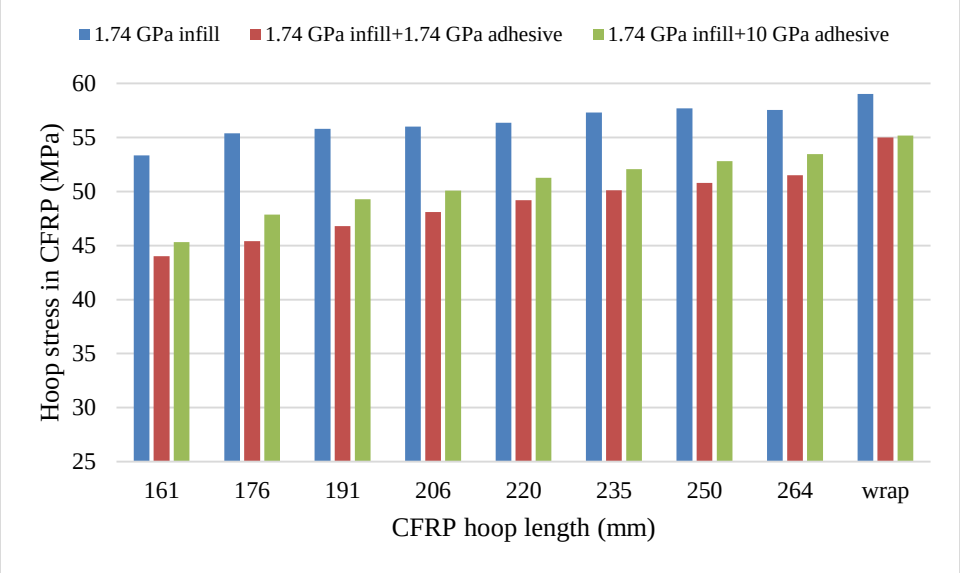

Figure 31 Effect of adhesive on hoop stress in pipe with infill material of 1.74 GPa epoxy

6.7 Effect of interface bonding condition

Ideally, the CFRP is bonded well with the steel pipe wall and there is no slip at the interface. However, if the interface bonding is not perfect, the performance of composite repair system is influenced. In this section, FE models with different interface bonding conditions were developed, including full bonding (no slippage allowed), frictional interface with friction coefficient of 1.0, and frictional interface with friction coefficient of 0.5. The thickness of the CFRP in the simulation was fixed at 6.2 mm. The CFRP patch with 220 mm in the hoop direction, and the CFRP wrap were simulated.

Figure 32(a) and (b) show the calculated maximum von Mises in the pipe wall and the maximum hoop stress in the CFRP under the MAOP, respectively. For both patch repair and wrap repair, the hoop stress in the CFRP and the von Mises stress in the pipe wall were similar as different friction coefficients were assumed at the interface. However, compared with the fully bonded condition, the fictional interface caused the decrease of hoop stress in CFRP but the increase of von Mises stress in the steel. This is reasonable because the allowance of slippage at the frictional interface reduces the stress transfer from steel to the CFRP. The stress values were found more sensitive to the interface condition for the patch repair, which is because the wrap repair requires less stress transfer at the interface. Therefore, it is more critical to have good bonding between CFRP and pipe wall to ensure the effectiveness of patch repair.

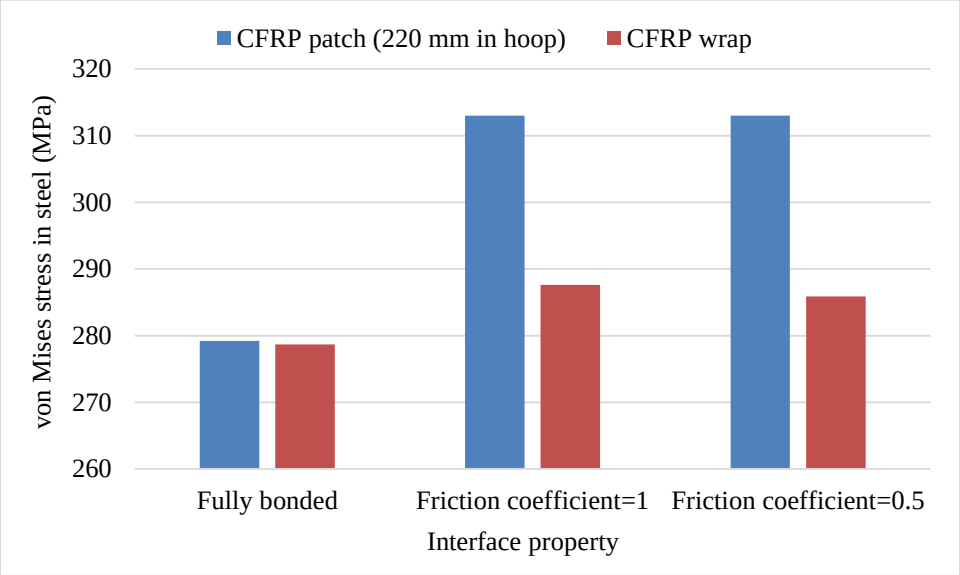

(a)

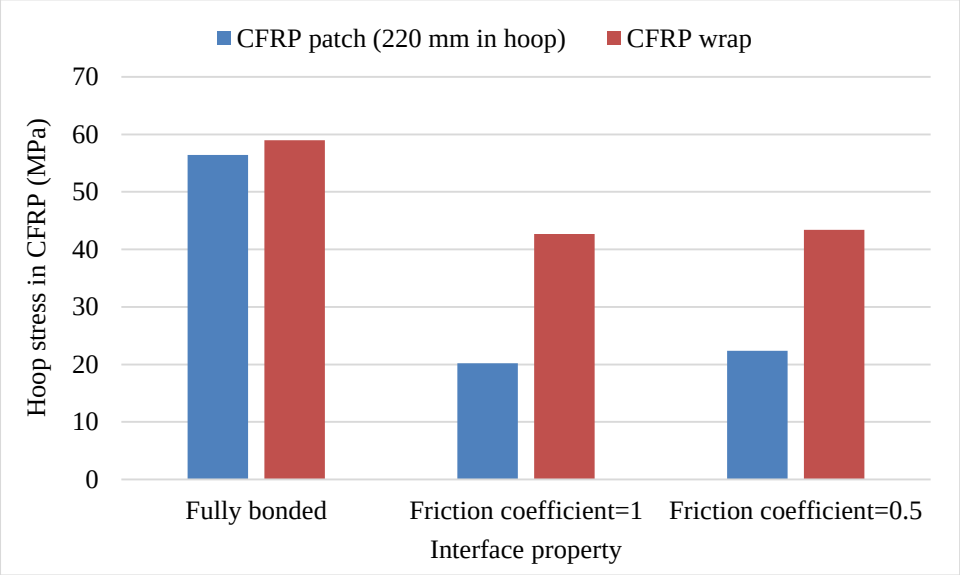

(b)

Figure 32 Effect of interface property on (a) von Mises stress in pipe, and (b) hoop stress in CFRP

Chapter 7 Findings and Recommendations

7.1 Findings

This study aimed order to develop an inorganic coating composite for corrosion protection and rehabilitation of pipeline in aggressive environments. The performance of inorganic coating was evaluated as corrosion barrier and strengthening system for composite repair of pipeline.

The inorganic composite coating was developed using alkali activation and microfiber. The coating will be in the class of geopolymeric material with zero CO2 and VOC emission. The coating has good adhesion with pipeline surface and abrasion resistance due to its inorganic nature. The addition of discrete micro-fiber could produce high strength with comparable strain with the metallic pipeline for repair of damaged pipeline. The greater surface activity of nano-particles can increase the density of coating, reduce the transport path of corrosive species, and enhance the protective performance.

Laboratory tests were conducted to examine the effects of nanomaterials on coating performance, including electrochemical measurement, durability evaluation, pull-off strength, and lap-shear test. A custom corrosion chamber was built to achieve an accelerated corrosion process including dry, fog spray, freezing, and UV radiation cycles. Among different nanomaterials used for coating modification, nano silica showed relatively better performance in terms of corrosion resistance and interface bonding with steel substrate. The observations for performance of nano-additives in terms of interface bonding strength were consistent with the corrosion resistance in accelerated corrosion tests. However, variations in performance were observed for the nano-modified coating, depending on coating thickness and the content of nanomaterial.

The inorganic coating can be used with CFRP for composite repair of pipeline. 3-D FE models to evaluate mechanical behavior of the pipeline with composite repair systems using carbon fiber reinforced polymer (CFRP). Two different repair strategies, namely wrap repair and patch repair were considered. The presented model was validated with experimental results reported in the literature. The analysis findings show that the patch repair can be used for composite repair of pipeline defects due to corrosion-induced thickness loss in the pipe wall. The maximum von Mises stress in the pipe wall and hoop stress in the CRFP are affected by the modulus of infill material and the adhesive layer between CFRP and pipe wall. The bonding condition between CFRP and pipe wall is critical to reduce the maximum stresses in the patch repair.

7.2 Recommendations

Geopolymer is one type of green materials that can be synthesized from silicate- and aluminate-bearing materials and even wastes at ambient. Geopolymerization process occurred by synthesizing aluminosilicate source materials with alkaline activator liquid to form hydrated product. The properties of geopolymer coating depend on the source and composition of raw materials. Therefore, future research need be conducted to identify the right combination of raw material for synthesization of coating matrix with desired properties.

On the other hand, hybrid coating is recommended to improve the performance of coating system for pipeline application. This could be achieved by using inorganic coating as primer and the organic coating as top layer to combine the advantages of both coatings.

References

49 CFR 192.619 - Maximum allowable operating pressure: Steel or plastic pipelines. Accessed at https://www.law.cornell.edu/cfr/text/49/192.619

American Society of Mechanical Engineers (ASME), (2006) Repair of pressure equipment and piping, ASME PCC-2–2006, New York

Alrudayni, M. (2015). "Evaluation of External Coating Performance on Buried Pipelines in the Oil and Gas Industry."Thesis

Ayaz, Y., Çitil, Ş., and Şahan, M. F. (2016). "Repair of small damages in steel pipes with composite patches." Materialwissenschaft und Werkstofftechnik, 47(5-6), 503–511.

Balaguru, P. N. and Lee, K.W. (2001). "Effectiveness of High Strength Composites as Structrual and Protective Coating for Structural Elements," Final Report NETCR 28, New England Transportation Consortium.

Balaguru, P.N. and Chong, K.P. (2005) Postponement of failure of concrete by surface protection and durability aspects, Proceeding of International Conference on Fracture, Italy.

Balaguru P. N. and Brownstein, J. (2008) Inorganic Protective Coatings and Fiber Reinforced Polymers Demonstration Project: Route 47 Wildwood Drawbridge Bridge House Rehabilitations, Final Report, FHWA-NJ-2008-013

Chan, P., Tshai, K., Johnson, M., Choo, H., Li, S., and Zakaria, K. (2014). "Burst strength of carbon fibre reinforced polyethylene strip pipeline repair system - a numerical and experimental approach." Journal of Composite Materials, 49(6), 749–756.

Chong, S.L. "A Comparison of Accelerated Tests for Steel Bridge Coatings in Marine Environments." Journal of Protective Coatings & Linings, vol. 14, no. 3, 1997

Cunha S.B., and Netto T.A. (2012). "Analytical solution for stress, strain and plastic instability of pressurized pipes with volumetric flaws." Int. J. Press. Vessels Pip., 89, 187-202.

Duell J.M., Wilson J.M., and Kessler M.R. (2008). "Analysis of a carbon composite overwrap pipeline repair system." Int. J. Press. Vessels Pip., 85, 782-788.

Égert, J., and Pere,B. (2009). "Repair of Internal and External Longitudinal Failures of Pipes by Fabric Composite Reinforcement."ActaTechnicaJaurinensis, 2(1).

Farrag, K. (2013). Selection of Pipe Repair Methods. Selection of Pipe Repair Methods, working paper, Gas Technology Institute, Des Plaines, Illinois.

Fawzia, S., Al-Mahaidi, R., and Zhao, X.L. (2006) "Experimental and finite element analysis of a double strap joint between steel plates and normal modulus CFRP." Composite structures 75(1): 156-162.

He, X., and Shi, X. (2009). “Self-repairing coating for corrosion protection of aluminum alloys.” Progress in Organic Coatings, 65(1), 37–43.

Kash, E. (2003). “The Mechanisms of Corrosion and Utilizing Fiber Reinforced Polymers as a Chloride Barrier.” 407 Town Engineering,1–12.

Kodumuri, P. and Lee, S.-K. (2012). Federal Highway Administration 100-year coating study. U.S. Dept. of Transportation, Federal Highway Administration, Research, Development, and Technology, Turner-Fairbank Highway Research Center, McLean, VA.

Lyon, R., Balaguru, P.N., Foden, A., and Sorathia, U. (1997) Fire Resistant Aluminosilicate Composites, Fires and Material, Vol. 21, 67-73

Majid, Z., Mohsin, R., Yaacob, Z., and Hassan, Z. (2010). “Failure analysis of natural gas pipes.” Engineering Failure Analysis, 17(4), 818–837.

Motta R. S., Cabral H.L.D., Afonso S.M.B., Willmersdorf R.B., Bouchonneau N., Lyra P.R.M., and de Andrade E.Q. (2017). “Comparative studies for failure pressure prediction of corrodedpipelines.” Eng. Fail. Anal., 81, 178-192.

Liu, Hongbo, et al. "Prediction of fatigue life for CFRP-strengthened steel plates." Thin-Walled Structures 47.10 (2009): 1069-1077

Mally, T. S., Johnston, A. L., Chann, M., Walker, R. H., and Keller, M. W. (2013). “Performance of a carbon-fiber/epoxy composite for the underwater repair of pressure equipment.” Composite Structures, 100, 542–547.

Najm, H., Secaras, J., and Balaguru, P.N. (2007) “Compression Tests of Circular Timber Column Confined with Carbon Fibers Using Inorganic Matrix”, Journal of Materials in Civil Engineering, ASCE, Vol.19, No.2, pp 198- 204.

Papakonstantinou C.G. and Balaguru, P.N. (2007) “Fatigue Behavior of High Temperature Inorganic matrix composites”, Journal of Materials in Civil Engineering,” ASCE, Vol.19, No.4, pp 321- 328.

Popoola, A., Olorunniwo, O., and Ige, O. (2014). “Corrosion Resistance Through the Application of Anti- Corrosion Coatings.” Developments in Corrosion Protection.

Ramakrishna, C., and Balu, J. K. (2017). “Finite Element Analysis of the Composite Patch Repairs of the Plates.” International Journal of Engineering Research and Applications, 07(02), 10–18.

Schad, M., and Zipffel, O. (2007). “Aspects of modern corrosion protective coating technology.” Pipeline Technology Conference 2007.

Schnerch, D. and et al. (2004) "Strengthening Steel Structures and Bridges with High-Modulus Carbon Fiber-Reinforced Polymers Resin Selection and Scaled Monopole Behavior." Transportation Research Record1892: 237-245.

Shamsuddoha, M., Islam, M. M., Aravinthan, T., Manalo, A., and Lau, K. (2012). Fiber Composites for High Pressure Pipeline Repairs, in-air and subsea – An Overview, APFIS2012.

Song, F., and Sridhar, N. (2008). "Modeling pipeline crevice corrosion under a disbonded coating with or without cathodic protection under transient and steady state conditions," Corrosion Science, 50(1), 70–83.

Tavakkolizadeh, M. and Saadatmanesh, H. (2001). "Galvanic Corrosion of Carbon and Steel in Aggressive Environments," Journal of Composites for Construction, 5(3):200-210

Toutanji, H.A., Zhao, L.,Deng, Y.,Zhang, Y. and Balaguru, P.N. (2006) "Cyclic Behavior of RC Beams Strengthened with Carbon Fiber Sheets Bonded by Inorganic Matrix", Journal of Materials in Civil Engineering, ASCE, Vol.18, No.1, pp.28-35, 2006

Theisen, S. A., and Keller, M. W. (2016). "Comparison of Patch and Fully Encircled Bonded Composite Repair," Conference Proceedings of the Society for Experimental Mechanics Series Mechanics of Composite and Multi-Functional Materials, Volume 7, 101–106.

Weiser, J. (2011) "Protect Underground Piping from Corrosion: What to Do before the Outage." Combined Cycle. (May 18, 2016)

Zhang, Z., Yao, X., and Wang, H. (2012). "Potential application of geopolymers as protection coatings for marine concrete III Field experiment," Applied Clay Science, Vol. 67-68, 57–60.